Advanced Photonic Measurements for Quantum Information

Brendon Lloyd Higgins, BSc. BInfTech

Submitted in partial fulfilment of the requirements of the degree of BSc. (Hons)

Faculty of Science, Griffith University

October 2006

Abstract

We investigate advanced quantum measurements by considering a combination of two advanced measurement schemes, namely quantum non-demolition (QND) and unambiguous state discrimination (USD). We attempt to create and demonstrate a proof-of-principle circuit that performs unambiguous non-demolition discrimination of non-orthogonal states.

QND is introduced as an operation to measure a system, in this case a qubit, in the logical basis without influencing the state of the system or destroying the information carrier. The controlled-NOT (CNOT) gate is described and shown to be capable of performing QND measurements by correlating the signal input state with the state of an ancilla system, called the meter. We then describe its use as a two-qubit entangling device and a weak QND measurement device. A non-deterministic implementation of a CNOT gate in the coincidence basis using polarised photons is presented. This circuit employs Hong-Ou-Mandel interference, which is also described, and has a $1/9$ probability of success.

USD is introduced as a mechanism to discriminate between two non-orthogonal states without error, and we describe its theoretical structure as a Positive Operator Valued Measure. The operation of an optical polarisation-based implementation of USD is presented and described. We consider USD functioning on entangled states resulting from a QND operation, and find that only considering meter output states gives equal statistics for both non-orthogonal input states, and is thus insufficient to determine anything about the state of the signal input.

However, it is found that the signal output is orthogonalised by the USD operation on the meter output, and that the state of the signal output can be used to determine the truth or falsehood of the USD measurement result. Three approaches are suggested to solve the issue of measuring the signal output while maintaining the condition of non-demolition. The first approach is to filter the output, conditional on the signal not being found to be in the state that indicates a false USD measurement, by way of a polarising beam splitter. The second approach is to perform a standard QND measurement on the orthogonalised signal. The third approach is to

use a CNOT-like device that converts the resulting states after the QND device into separable states.

The described CNOT and USD circuits are constructed and characterised. The CNOT circuit is built and its truth table found to have a fidelity of 0.93. It is then shown to exhibit entangling of two unentangled qubits, with tangle 0.53 ± 0.06 and fidelity 0.81 ± 0.02. The USD circuit is also built and tested with states 45° apart and found to be working with less than 6% error in inconclusive results, and less than 2% error in discriminated states.

The two circuits are then combined and unambiguous non-demolition state discrimination is performed on the same pair of 45° separated states. State tomography is performed on the signal output for each USD measurement result for each input state to construct density matrices representative of the final state of the signal. This is in order to measure the correlation between the two systems. Purities of greater than 90% were typically found, and trace distances from expected results of less than 0.2 were common, after correcting for photon source imperfections.

Weak QND measurements are attempted on the same non-orthogonal states in the same way as weak QND measurements are performed on orthogonal states. It was found that this approach was insufficient to successfully perform weak QND measurements.

We discuss the limitations of our demonstration, and consider future directions, such as the implementation of more efficient filters.

Finally, we conclude that we have successfully constructed a proof-of-concept demonstration of a quantum circuit which performs unambiguous non-demolition discrimination of non-orthogonal optical polarisation states.

Contents

List of Figures

List of Tables

Acknowledgements

Thanks to my supervisor Geoff Pryde for his extensive help, explanations, persistence, and for spending what I'm sure totalled too many late nights thinking about various experiment related problems and mercilessly reviewing drafts of this thesis.

Big thanks to Andrew White of the University of Queensland for lending us space and equipment in his QT lab for the duration of the experiment, while Geoff's new lab at Griffith University was being set up. Thanks also for being so gracious when we stayed longer than we had originally anticipated.

Many thanks must also go to Ben Lanyon, my UQ collaborator for this experiment, who helped a great deal in understanding and setting up the experiment, maintaining the source, and tracking down problems we were having in the lab with unexpected results and over-enthusiastic air-conditioning.

As well, thanks to all the guys in the lab, particularly Till Weinhold, Kevin Resch, Rohan Dalton, Nathan Langford, and Geoff Gillett, for their help, discussions, and advice. Thanks also to Tim Ralph for discussions about the circuit and its future directions.

This work has not previously been submitted for a degree or diploma in any university. To the best of my knowledge and belief, the dissertation contains no material previously published or written by another person except where due reference is made in the dissertation itself.

Brendon Higgins

Chapter 1

Introduction

The bizarre, counter-intuitive nature of quantum mechanics has engrossed physicists since its discovery at the dawn of the 20th century. Extrapolations of quantum theory to the macroscopic world, such as the Schrödinger's cat thought experiment, betray the strange properties of quantum interaction and measurement that seem to defy what common sense has taught us.

It has only been in the last few decades that technology has improved to the state where the theory of quantum mechanics has been usefully applied outside the lab. All modern electronics, imperative in first-world economies and lifestyles today, employ forms of applied quantum theory, without which they would not operate. With quantum theory-based nanotechnology showing promise for new applications, the use of the principles of quantum mechanics in development of consumer products will become yet more prevalent.

The use of fundamental concepts of quantum theory in the field of information processing embodies the heart of quantum information. There is ever-increasing evidence that devices designed to process information using these fundamentals of quantum mechanics have an enormous potential. Already there is keen interest from governments, militaries and corporations in devices employing quantum encryption schemes [1], mechanisms for encrypting and transmitting information that are *physically* uncrackable.

Computation devices employing quantum mechanical principles such as superposition and entanglement have the potential to solve certain problems up to exponentially faster than is possible using any classical computation system [2]. Such problems include factorising large numbers, searching, and

simulation of quantum systems. As the young field of quantum algorithms grows, other applications for which quantum computers will yield an improvement may be discovered.

Quantum devices employing photons as the conveyor of quantum information are particularly interesting. Light has the advantage of having relatively little interaction with the environment and low decoherence rates when compared to other methods such as nuclear magnetic resonance. Also, light is often thought of as the best carrier of information due to its speed and relative lack of crosstalk, and we already see this application in telecommunications as fibre optic cables and radio transmissions. Since light is well suited to information transfer, it is natural to investigate how far we can extend the application of light into information processing, as a way of eliminating any inefficiencies inherent in conversion to and from the information carriers of other kinds of processing systems.

A key area of quantum mechanics is measurement theory. Understanding of measurements will be important for future quantum computing devices and quantum communications protocols. Quantum encryption schemes, for example, are based on the fundamental property of quantum mechanics that a measurement of a system necessarily affects the outcome of future measurements. This property of quantum measurement also allows measurements to be used to control the evolution of quantum systems, leading to quantum computation schemes ([3] and [4] for example) where measurement not only allows the inspection of results, but actually plays a fundamental role in the operation of the computer.

Quantum measurement devices also have application outside the realm of quantum information systems. Logical circuit elements developed for quantum information processing may make good devices for the measurement of certain quantum mechanical systems in contexts unrelated to quantum computing. This crossover of ideas demonstrates the power of the field of Quantum Information Science.

We commonly think of quantum measurements as projective measurements, where the act of measuring a system causes the system to collapse to either the state we are measuring against, or alternatively to the orthogonal of that state. In essence, the results we obtain from such a measurement constitute a succeed or fail answer when we attempt to project the system onto a state. Quantum measurement theory allows for much more general

kinds of measurements, however. Quantum mechanics allows nonprojective measurements, such as measurements with more than two possible results, and indirect measurements.

It is important to explore the limits of quantum measurement, including finding out how general quantum measurements can be and how we might implement them. There are a number of schemes that go beyond standard projective measurements, two important examples and the focus of this thesis being quantum non-demolition (QND) [5] measurements and unambiguous state discrimination (USD) [6].

QND measurements allow the state of a quantum system to be measured without destroying the system in the process. This is particularly useful for photonic systems where the usual method of measure requires the absorption of the photon in a photo-sensitive material, thus destroying it. By QND, we are able to determine the state of the information carrier (the photon) without destroying the carrier itself. Furthermore, when a QND measurement is performed on a two-level system (a qubit) that is in the *logical* basis, the state of the system is left undisturbed, meaning a photon in a logical state can be measured and then continue to another part of the quantum circuit as if it had not been measured at all. QND devices also have the capacity to perform *weak* measurements, where a trade-off is made between the amount of back-action caused on states that are not in the logical basis and the amount of information gained in the measurement.

USD is a solution to the problem of determining, without error, the state of a system which may be in one of two non-orthogonal states. It is a non-orthogonal measurement and so it is different from a projective measurement in a given basis. Where an attempt to discriminate non-orthogonal states using a projective measurement will sometimes produce a conclusive and wrong result, USD will always yield a correct result whenever it does not yield a third inconclusive result. USD is an example of a class of measurements called *Positive Operator Valued Measures* or POVMs. This particular POVM has application in understanding how an eavesdropper might try to attack a quantum communications channel, but is also interesting as a simple example of POVMs generally.

We wish to explore further generalising measurements beyond QND measurements and standard implementations of POVMs. While this is a very broad category of measurements, by investigating what happens when we

combine QND and USD, we get some insight into a number of key issues in the area. We choose USD because it is a relatively simple example of a POVM.

QND devices have been realised experimentally [7, 8], as have USD devices [6, 9]. Our experiment attempts to build upon those implementations by combining them. The aim is to design and implement a device that can non-destructively and unambiguously distinguish an input state of being one of two possible non-orthogonal quantum states. This not only will allow us to investigate an example of extended general measurements, but it also has possible applications, including as an eavesdropping device which we can compare to other schemes, and error correction in certain contexts.

There is more than one way to go about combining these two devices. The first and perhaps most obvious way is to simply perform the entangling step of a QND measurement, where the signal and meter systems become correlated, but instead of performing a projective measurement on the meter, perform a USD measurement. This method works well in limited cases, but as it turns out, even in the ideal case of no experimental loss and a deterministic QND device, it only successfully performs QND 50% of the time (the other 50% being filtered away). This can be seen as the first step towards an unambiguous non-demolition discrimination device.

This method introduces some back-action on the input due to the non-orthogonal states not being in the orthogonal logical states. As such, it requires feed-forward in a full implementation to ensure the state of the input is preserved.

An alternative method is to implement two QND-like devices, one before the USD device, and one after. While in principle such a device would work well, in the ideal case 100% of the time is possible, such a device requires many more components (aligned and calibrated), and thus is difficult to construct successfully. This would then be the next step towards a non-demolition USD device.

Since this experiment is a proof-of-concept to allow us to examine key issues of extensions of general measurements, we have chosen to implement the first method, instead. However, we are also able, from our experimental results, to test whether the second method works in principle.

The operation of the QND-USD device requires two inputs in order to work — the system we wish to measure, and an ancilla. If we consider the

second system not as an ancilla but as a the second part of a two-system input we wish to measure, then the device can be thought of as an advanced 2-qubit POVM. Although it is not immediately obvious what application this *particular* two-qubit POVM might have, it nevertheless differs markedly from standard two-qubit measurement, which is a separate projective measurement on each of the two qubits. It is both an entangling measurement and a six-outcome measurement, whereas a standard projective measurement is an unentangled, four-outcome measurement.

The following sections present the theory underpinning, construction of, results from and characterisation of our experimental realisation of both independent and combined implementations of QND and USD in optics. The QND device is implemented using a quantum logic gate called a *CNOT* gate. CNOT gates, though conceptually simple, have remarkable power. They can be used in the implementation of a number of advanced measurement schemes including QND, weak measurement, and Bell state measurement. The optical CNOT circuit we plan to implement is non-deterministic, with $1/9$ probability of success.

We then take the first step, combining the QND and USD circuits so that unambiguous state discrimination is performed on the result of the QND. We show in-principle demonstrations of the circuit, and characterise the states it produces. Since the USD operation is a kind of filtering, the circuit can also be configured to produce orthogonal maximally-entangled states from unentangled inputs — a kind of *controlled*-nonunitary operation.

This combined QND-USD apparatus has allowed us to perform one of the most general quantum measurements to date: we have used it to demonstrate a non-destructive non-projective measurement on a single qubit, we are currently undertaking work to show a kind of controlled nonunitary operation, and we have noted its extension to future generalised measurement technologies.

Chapter 2

The CNOT Gate

2.1 From NAND And NOR To CNOT

The fundamental components that make up classical computer systems are bits and binary logic gates. A bit is a base 2 digit, taking the values 0 or 1, that is the fundamental unit of information which a computer can process. A binary logic gate is a device that takes one or two bits as inputs, performs some logical operation, and produces one or two bit outputs. Table 2.1 illustrates the actions of some common binary gates.

By connecting an output of one binary gate, making copies, and giving them as inputs to other gates, the flow of bit states through these gates is used to perform computations. More gates chained together in this way on an integrated circuit can perform more complex operations, and with the addition of timing devices, they can be made to iteratively execute complicated algorithms. This is basically how almost all computers operate today.

In practice, most integrated circuit systems using binary logic are constructed from a large number of only a single kind of logic gate, either *NAND* or *NOR*. Remarkably, these gates can be used to construct any binary logic gate provided that copies of input states can be made and ancilla states are available [10]. Because of this special property they are known as *universal* gates. Though NOR gates can be used just as well, we consider the NAND gate.

A NAND gate is equivalent to an AND gate with a NOT operation on the output bit. Its output is 0 only when both inputs are 1, as shown in its

(a) The NOT gate.

Input	Output
0	1
1	0

(b) The AND gate.

Input 1	Input 2	Output
0	0	0
0	1	0
1	0	0
1	1	1

(c) The OR gate.

Input 1	Input 2	Output
0	0	0
0	1	1
1	0	1
1	1	1

(d) The XOR gate.

Input 1	Input 2	Output
0	0	0
0	1	1
1	0	1
1	1	0

Table 2.1: Truth tables of common binary gates in classical computers. When the gates are supplied with the listed input(s), they give the corresponding output(s). Typically, binary gates only supply one output. A NOT gate takes only one input, while the AND, OR, and XOR gates take two inputs.

Input 1	Input 2	Output
0	0	1
0	1	1
1	0	1
1	1	0

Table 2.2: NAND truth table. For a given pair of inputs, the gate suppies the corresponding output.

truth table, Table 2.2. Figure 2.1 shows how all other binary logic gates can be constructed from NAND gates.

Analogous to the components of classical computer systems, quantum computer systems are often comprised of qubits and quantum gates. Qubits are similar to bits in that they are two-level systems that can have logical states of 0 or 1, but as they are quantum mechanical objects, they possess the ability to be in superposition states of 0 and 1. Quantum gates are like binary logic gates but perform operations on qubits. Because of the increase in state-space size qubits provide, quantum gates must be able to perform more complicated operations than binary logic gates.

For classical computation systems both conditions, the availability of ancilla bits and the ability to copy unknown states (known as a *Fan-out*

$$
\begin{aligned}
\neg A &= A|A \\
A \wedge B &= (A|B)\,|\,(A|B) \\
A \vee B &= (A|A)\,|\,(B|B) \\
A \oplus B &= (A|\,(A|B))\,|\,(B|\,(A|B))
\end{aligned}
$$

Figure 2.1: Construction of binary logic operators from NAND gates, where | represents the NAND operation, $\wedge$ represents the AND, $\vee$ the OR, and $\oplus$ the XOR operations. All binary gates in classical computers can be assembled using combinations of NAND gates and bit copying.

operation), are easily satisfied. However for quantum computation systems, due to the no-cloning theorem, quantum states cannot be copied [2]. This means that quantum gates cannot be built from the same universal gates as classical logic gates.

For a quantum system there exists a combination of qubit gates which, like a NAND gate and Fan-out in a classical system, turns out to be universal. This is the combination of unitary single-qubit gates, and the *CNOT* gate. Like the NAND and NOR gates, there is more than one combination of qubit gates that is universal — there are, in fact, an infinity of them — however the CNOT gate and unitary single-qubit gates are the most commonly considered.

Unitary single-qubit gates take a qubit from one state to another in a predictable fashion, an example being the quantum bit-flip gate, which performs the same action on qubits in logical states 0 or 1, as a classical NOT gate on bits 0 and 1[1]. These gates are much easier to create since they only work on single qubits, whereas the CNOT gate implements an interaction between two qubits.

Like a NAND gate, a CNOT gate takes two inputs, the *target input* and the *control input*, but unlike NAND it gives two outputs, the *control output* and the *target output*. Although the proof is more complicated, CNOT gates, combined with single qubit gates, can perform any unitary qubit transformation, and thus they can be used to construct any quantum circuit. In this regard they are universal [2].

The gate's name is a clue to its function: CNOT stands for 'Controlled

[1]Indeed, it could even be argued that the NOT gate is in fact the classical limit of the quantum bit-flip gate.

Input		Output	
Control	Target	Control	Target
0	0	0	0
0	1	0	1
1	0	1	1
1	1	1	0

Table 2.3: CNOT truth table for logical states. For the given pair of logical inputs, a CNOT gate will supply the corresponding pair of outputs.

Not', and is essentially a controllable form of a simple inversion of a qubit state, similar to but more general than the NOT binary gate. It actually behaves much like a classical XOR (exclusive or) gate, as its truth table Table 2.3 demonstrates[2]. For a control input qubit of 0, the target output qubit is the same as the target input qubit. But for a control input qubit of 1, the target output is the *logical opposite* of the target input. In both cases the control output is the control input unchanged.

2.2 Operation Of The CNOT Gate

As the CNOT gate is a quantum gate it is able to perform operations on inputs beyond those in the logical 0/1 basis that the truth table shows. In order to get a better idea of what a CNOT does to superposition states, we will consider the operation of a CNOT more formally using Dirac notation and vector state representation.

Let the control input qubit state be represented by $|C\rangle$ and the target input $|T\rangle$. $|0\rangle$ and $|1\rangle$ are the 0 and 1 logical basis states, respectively. The control and target qubits can be any linear combination of $|0\rangle$ and $|1\rangle$, so the control and target two-qubit system can be represented as

$$|C\rangle \otimes |T\rangle = |CT\rangle = \alpha\,|00\rangle + \beta\,|01\rangle + \gamma\,|10\rangle + \delta\,|11\rangle$$

where α, β, γ, and δ are an arbitrary set of normalised complex parameters.

[2]Similar to the relationship between the quantum bit-flip and classical NOT gates, it could be argued that XOR is, in fact, a CNOT gate acting on classical states.

Represented in state vector form, this is

$$|CT\rangle = \begin{bmatrix} \alpha \\ \beta \\ \gamma \\ \delta \end{bmatrix}$$

The CNOT gate can be represented in matrix operator form as [2]

$$\hat{M}_{\text{CNOT}} = \begin{bmatrix} 1 & 0 & 0 & 0 \\ 0 & 1 & 0 & 0 \\ 0 & 0 & 0 & 1 \\ 0 & 0 & 1 & 0 \end{bmatrix}$$

in the $|0\rangle$ and $|1\rangle$ basis.

As is easily shown, applying the CNOT gate operation to the system we get

$$\hat{M}_{\text{CNOT}} |CT\rangle = \begin{bmatrix} 1 & 0 & 0 & 0 \\ 0 & 1 & 0 & 0 \\ 0 & 0 & 0 & 1 \\ 0 & 0 & 1 & 0 \end{bmatrix} \begin{bmatrix} \alpha \\ \beta \\ \gamma \\ \delta \end{bmatrix} = \begin{bmatrix} \alpha \\ \beta \\ \delta \\ \gamma \end{bmatrix}$$

and so

$$|CT\rangle \xrightarrow{\text{CNOT}} \alpha |00\rangle + \beta |01\rangle + \delta |10\rangle + \gamma |11\rangle$$

The γ and δ parameters have swapped the states to which they correspond; the α and β parameters have not changed.

By setting α, β, γ, and δ to certain particular values, we can show that this does indeed work as the truth table above describes. For example, consider an input state of $|CT\rangle = |10\rangle$. Here, the control qubit is in the logical 1 state and the target in the logical 0 state. The parameters must be $\alpha = \beta = \delta = 0$ and $\gamma = 1$. Then it becomes obvious that the output state is $|11\rangle$, i.e. the control qubit remains in the logical 1 state, but the target qubit has flipped to the logical 1 state, which is exactly what we expected.

Another interesting example of the CNOT is with the control input not in one of the logical basis states, but in a superposition. Consider the target input in the $|0\rangle$ state and the control input in the $\frac{1}{\sqrt{2}}(|0\rangle + |1\rangle)$ superposition

state. It can be shown that this produces the output

$$|CT\rangle = \frac{1}{\sqrt{2}}\left(|00\rangle + |11\rangle\right)$$

which is a maximally entangled Bell state. This demonstrates that the CNOT gate can be used to produce entangled states from unentangled inputs. It also demonstrates the fact that when applying the CNOT with a control input that is not in the logical basis, the control output may not be the same as the input.

2.3 CNOT And CSIGN

A quantum gate closely related to the CNOT is the *CSIGN* gate. Like the CNOT, the CSIGN performs an operation on a target qubit conditional on a control qubit. Specifically, a CSIGN changes the sign of the amplitude of the $|11\rangle$ term of the general input state $|CT\rangle = \alpha\,|00\rangle + \beta\,|01\rangle + \delta\,|10\rangle + \gamma\,|11\rangle$.

A CSIGN performs the operation

$$|CT\rangle \xrightarrow{\text{CSIGN}} \alpha\,|00\rangle + \beta\,|01\rangle + \delta\,|10\rangle - \gamma\,|11\rangle$$

which can be represented by

$$\hat{M}_{\text{CSIGN}} = \begin{bmatrix} 1 & 0 & 0 & 0 \\ 0 & 1 & 0 & 0 \\ 0 & 0 & 1 & 0 \\ 0 & 0 & 0 & -1 \end{bmatrix}$$

We can show that a CSIGN and unitary single-qubit gates can be used to construct a CNOT gate, indeed this is how a CNOT is achieved in our experiment. A unitary single-qubit operation that rotates a qubit state by 45°, for example, taking $|0\rangle$ to $\frac{1}{2}\left(|0\rangle + |1\rangle\right)$, is called a Hadamard gate. This gate is used to operate on $|T\rangle$ before and $|T'\rangle$ after the CSIGN. A Hadamard gate can be represented in matrix form

$$\hat{H} = \frac{1}{\sqrt{2}} \begin{bmatrix} 1 & 1 \\ 1 & -1 \end{bmatrix}$$

In a two qubit system $|CT\rangle$, applied to only the target qubit $|T\rangle$, the matrix

becomes the tensor product $\hat{H}_T = \hat{\mathbb{1}} \otimes \hat{H}$, i.e.

$$\hat{H}_T = \frac{1}{\sqrt{2}} \begin{bmatrix} 1 & 1 & 0 & 0 \\ 1 & -1 & 0 & 0 \\ 0 & 0 & 1 & 1 \\ 0 & 0 & 1 & -1 \end{bmatrix}$$

Then, the operation of applying the Hadamard to the target qubit, performing the CSIGN, and applying the Hadamard to the target qubit again is

$$\begin{aligned}
&\hat{H}_T \, \hat{M}_{\text{CSIGN}} \, \hat{H}_T \\
&= \frac{1}{2} \begin{bmatrix} 1 & 1 & 0 & 0 \\ 1 & -1 & 0 & 0 \\ 0 & 0 & 1 & 1 \\ 0 & 0 & 1 & -1 \end{bmatrix} \begin{bmatrix} 1 & 0 & 0 & 0 \\ 0 & 1 & 0 & 0 \\ 0 & 0 & 1 & 0 \\ 0 & 0 & 0 & -1 \end{bmatrix} \begin{bmatrix} 1 & 1 & 0 & 0 \\ 1 & -1 & 0 & 0 \\ 0 & 0 & 1 & 1 \\ 0 & 0 & 1 & -1 \end{bmatrix} \\
&= \frac{1}{2} \begin{bmatrix} 1 & 1 & 0 & 0 \\ 1 & -1 & 0 & 0 \\ 0 & 0 & 1 & 1 \\ 0 & 0 & 1 & -1 \end{bmatrix} \begin{bmatrix} 1 & 1 & 0 & 0 \\ 1 & -1 & 0 & 0 \\ 0 & 0 & 1 & 1 \\ 0 & 0 & -1 & 1 \end{bmatrix} \\
&= \frac{1}{2} \begin{bmatrix} 2 & 0 & 0 & 0 \\ 0 & 2 & 0 & 0 \\ 0 & 0 & 0 & 2 \\ 0 & 0 & 2 & 0 \end{bmatrix} \\
&= \hat{M}_{\text{CNOT}}
\end{aligned}$$

The fact that a CNOT gate can be described in terms of a CSIGN and Hadamard gates indicates that the CSIGN gate, with unitary single-qubit gates, also acts as a universal qubit gate.

2.4 A QND Measurement Device

One use of a CNOT is as an apparatus to perform a quantum non-demolition (QND) measurement on a single qubit. QND is a measurement on a quantum system in which the effect of the necessary back-action on the system is restricted to unwanted observables [5]. A QND measurement satisfies the

three conditions:

1. It produces a result correlated to the observable being measured,
2. It does not alter the observable being measured, and
3. Repeated measurements produce the same result.

In reference to quantum optics, an important point is that QND allows for the measurement of a photonic system without destroying the photon that comprises it. Often in quantum optics in order to measure the state of a system, the system will be destroyed. For example, to measure the polarisation of a single photon, that photon must be distinguished by a polariser and then absorbed by a photo-detector. An optical QND device would allow its users to perform a polarisation measurement on the photon while allowing that photon to continue travelling to another part of the quantum circuit.

The way to achieve a QND measurement is generally as follows [5]: The system the experimenter wishes to measure, the *signal* S, is entangled sufficiently with another system, the *meter* M, such that information about S can be derived by a destructive measurement of M. This leaves S intact while gaining information about its state.

The way a CNOT can perform a QND measurement on a qubit is by preparing, as the meter M, the target input in state $|0\rangle$, and passing the signal S as the control input. When $|S\rangle$ is a logical state, $|0\rangle$ or $|1\rangle$, the CNOT operation causes $|M'\rangle$, the meter output, to equal $|S\rangle$. Then it is easy to see how a destructive measurement performed on M' will give the same result as if a measurement was performed on S, while leaving S itself intact.

Since a CNOT gate can be used to implement a QND device the terms "signal" and "meter" are sometimes used interchangeably with "control" and "target".

It appears that through this QND measurement a copy of S is being made, but this is not strictly true. When the signal is in a logical state, a copy of that state is indeed made in the meter. This is the regime in which QND works. However, for general S states this is not the case, and the integrity of the no-cloning theorem for general states [2] is preserved.

Consider S the signal in some arbitrary unknown state, $|S\rangle = \theta\,|0\rangle + \phi\,|1\rangle$. With these conditions the CNOT will take the meter (target) from $|M\rangle = |0\rangle$

and the signal (control) $|S\rangle$ to an entangled state $|S'M'\rangle = \theta\,|00\rangle + \phi\,|11\rangle$. If M' is then measured destructively, both $|S'\rangle$ and $|M'\rangle$ collapse to a result, the same result, in the same way as if S was measured destructively. Once this is done, the M' system no longer exists — it was destroyed in the act of measurement — but the S' system remains.

It is important to understand that no independent copy is made of S. We can see that what is created in the QND process is not a copy by considering the result of an actual copy operation (if one existed). If a copy was made of the unknown state $|S\rangle$ the result would have to be $|S'M'\rangle = |S\rangle \otimes |S\rangle = \theta^2\,|00\rangle + \theta\phi\,|01\rangle + \theta\phi\,|10\rangle + \phi^2\,|11\rangle$, which is not the result produced by the CNOT.

Instead of copying, S and the ancilla qubit M are *entangled*. When a destructive measurement is performed on M', both the states $|S'\rangle$ and $|M'\rangle$ collapse simultaneously to the same state. The back-action of QND measurement of signal states outside the logical regime changes the signal state. $|S'\rangle$ cannot be unentangled from $|M'\rangle$, and thus an independent copy can never be made using a QND arrangement, satisfying the no-cloning theorem.

This meets all the requirements of a QND measurement. The results are correlated, it does not alter the observable, and repeated measurements will produce the same result.

2.5 A Weak Measurement Device

The example above illustrates a *strong* QND measurement. Full state information is gained by this QND process. More interesting results of using a CNOT as a QND device can be obtained by considering superposition inputs of the meter M. For example, suppose instead of $|M\rangle = |0\rangle$ we use $|M\rangle = |+\rangle = \frac{1}{\sqrt{2}}\,(|0\rangle + |1\rangle)$. Then with an arbitrary signal state $|S\rangle = \theta\,|0\rangle + \phi\,|1\rangle$,

$$\begin{aligned} |SM\rangle \quad &= \quad \frac{\theta}{\sqrt{2}}\,|00\rangle + \frac{\theta}{\sqrt{2}}\,|01\rangle + \frac{\phi}{\sqrt{2}}\,|10\rangle + \frac{\phi}{\sqrt{2}}\,|11\rangle \\ &\xrightarrow{\text{CNOT}} \quad \frac{\theta}{\sqrt{2}}\,|00\rangle + \frac{\theta}{\sqrt{2}}\,|01\rangle + \frac{\phi}{\sqrt{2}}\,|11\rangle + \frac{\phi}{\sqrt{2}}\,|10\rangle \\ &= \quad |SM\rangle \end{aligned}$$

This has produced no correlation between S and M, so no information about S can be obtained by measuring M.

By varying the state of M from $|0\rangle$ to $|+\rangle$ we can produce output states with a continuum of correlation, from none to maximal correlation. By performing measurements on the meter qubits in these states we can obtain *partial* information about a system. These are known as *weak* measurements. As $|M\rangle$ varies from $|0\rangle$ to $|+\rangle$, the correlation diminishes from complete correlation to no correlation, and so measurements on the meter go from completely representative of the signal, to completely unrepresentative of the signal [11].

The key point of weak QND measurements is that, for signals that are not in one of the logical states, the amount of correlation and thus the amount of information obtained by a weak measurement is related to the degree that back-action affects the signal. For example, with a strong QND measurement, a signal in the state $|+\rangle$ becomes a maximally-entangled Bell state by the CNOT gate, and collapses to either $|0\rangle$ or $|1\rangle$ when the meter is measured. For a very weak measurement, the entanglement is greatly reduced. Measurement of the meter then results in little information, but the signal is left very near its original $|+\rangle$ state.

Because of this adjustable trade-off between information and back-action, the weak QND process has applications in eavesdropping and error correcting of optical communications, quantum control of a system by repeated measurement, feedback — anywhere where it might be useful to obtain partial information about a system while minimising the back-action.

Chapter 3

Optical Realisation Of A CNOT Gate

Using an optical CNOT gate for non-demolition measurements of photonic qubits was demonstrated by Pryde et al [8], and we follow the same procedure here. We work in the regime of photon polarisation encoded qubits, where we define a horizontally polarised photon (H) as being the logical state $|0\rangle$ (say), and a vertically polarised photon (V) as being the logical state $|1\rangle$ (say).

To control the polarisation state of individual photons we employ a combination of half-wave plates (HWPs) and quarter-wave plates (QWPs). A HWP rotates the polarisation state vector by 180° on the Poincaré sphere (the polarisation analogue of the Bloch sphere) around an axis defined by the wave plate crystal's own rotation relative to its optic axis. A HWP allows conversion between states of different linear polarisations. A QWP, which rotates vectors on the Poincaré sphere by 90°, allows conversion of linear polarisation to elliptical polarisation. A combination of quarter-, half-, then quarter-wave plates allows an arbitrary state to be arbitrarily rotated on the Poincaré sphere[1].

The experimental setup of the CNOT gate follows that of O'Brien et al [7], which is a simplification of the measurement-induced nonlinearity-based scheme of Knill, Laflamme, and Milburn [3]. The CNOT works by splitting each of the control and target photons into two modes, and performing a

[1]When starting or ending with with a linear polarisation, only a HWP and one QWP are required.

Hong-Ou-Mandel interference [12] between one mode of each photon, before interferometrically recombining the modes. It is heralded by coincident detection of the photons at the output, and works successfully with a probability of 1/9. This type of gate can operate with high fidelity [13].

It should be emphasised that since the CNOT gate is non-deterministic, its use as a QND device is an *in principle* application — a deterministic QND device would be desirable. In principle, it is possible to construct a deterministic linear optics CNOT gate using the ideas of measurement-induced nonlinearity that underlie this device [3], although such a device is not practically realisable yet.

3.1 Hong-Ou-Mandel Interference

Before we examine the CNOT circuit we should consider the quantum interference necessary for its operation. Hong-Ou-Mandel (HOM) interference is a purely quantum mechanical phenomenon that arises when two photons are coincident on the surface of a beam splitter such that the paths of the photons beyond the splitter are indistinguishable, that is, when it is impossible to determine which of two incoming photons follow one of two output paths. This indistinguishability between the two arms determines the degree to which HOM interference is observed. When the two beams are perfectly indistinguishable the number of coincident photons, one in each of the two outgoing paths, drops to zero.

A graph can be made of coincidences as distinguishability between photons is varied, say by changing the difference in arrival time at the beamsplitter. A dip in the graph can be seen around the point where the two beams become indistinguishable. The shape of the dip in the graph is related to the spatial overlap of the two photons. For Gaussian-shaped beams (the beams we will be using) the shape of the graph is also Gaussian, and ranges from some maximum number of coincidences outside the beam-overlap region, to 0 coincidences at the point of total indistinguishability. Figure 3.1 shows this idealised HOM-dip as a function of one degree of freedom for a pair of Gaussian beams. The width of the dip is a function of the coherence length of photons [12].

The HOM dip is due to destructive interference of the two possible output modes for which a coincidence occurs [14]. To understand why this occurs,

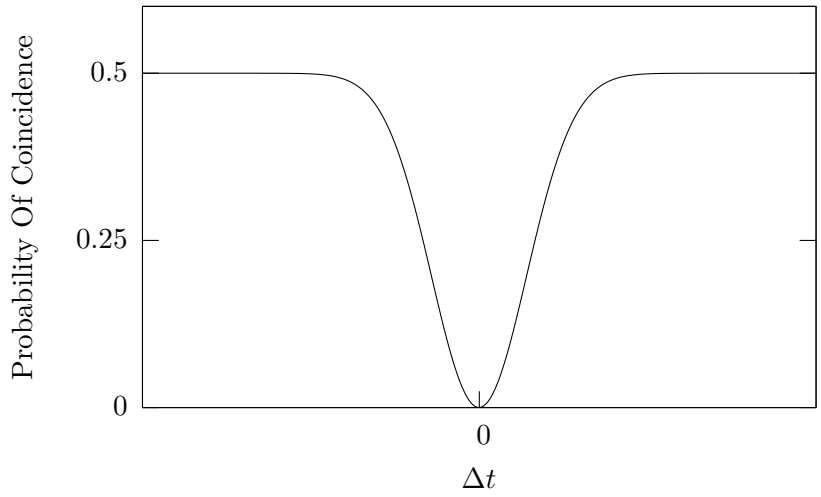

Figure 3.1: Ideal Hong-Ou-Mandel interference. As distinguishability of photons varies so does the rate of coincidence counts. In this example, the modes of photons at the beam splitter differ only in arrival times. As the difference in arrival times decreases the number of coincidence counts drops due to Hong-Ou-Mandel interference. In this ideal case, the number of coincidences when all degrees of freedom are identical is zero.

consider a beam splitter with reflectance r and transmittance t at which two coincident photons interfere as in Figure 3.2. A pair of photons travels towards the beam splitter in the input arms a and b. This can be represented in the photon number basis using creation operators as

$$|\psi_{\text{in}}\rangle = |11\rangle_{a,b} = \hat{a}_a^\dagger \hat{a}_b^\dagger |00\rangle_{a,b}$$

where $\hat{a}_x^\dagger$ is the creation operator on mode x. Note here that $|0\rangle$ and $|1\rangle$ do not represent logical qubit states, but 0 and 1 photons, respectively.

To find $|\psi_{\text{out}}\rangle$ we must consider the beam splitter transformation. The beam splitter takes a photon in the a input mode, and sends it to the c output mode with amplitude t, and to the d output mode with amplitude r. By the conservation of energy the process must introduce a π phase difference between the two outgoing beams [15]. We can achieve this constraint without loss of generality by assuming a $\pi/2$ phase shift upon reflection, so the component of amplitude due to reflection in modes c and d becomes

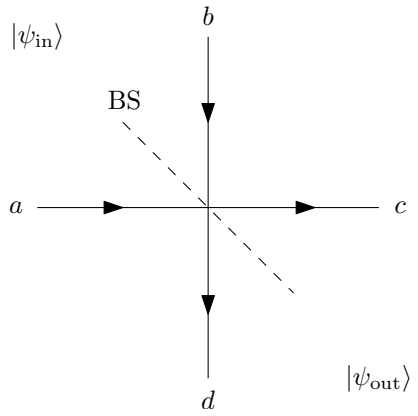

Figure 3.2: Beam splitter with simultaneous inputs, whose output modes perfectly overlap. One photon in the a path and one photon in the b path travel towards the 50:50 beam splitter. If the two photons arrive at the surface of the beam splitter at the same time, HOM interference causes them to pair up, with both photons leaving the beam splitter in either the c or d modes, but never one photon in each.

$e^{i\pi/2}r = ir$. We then have the beam splitter transformation equations

$$\begin{aligned} \hat{a}_a^\dagger &\rightarrow t\hat{a}_c^\dagger + ir\hat{a}_d^\dagger \\ \hat{a}_b^\dagger &\rightarrow ir\hat{a}_c^\dagger + t\hat{a}_d^\dagger \end{aligned}$$

We then find that as $|\psi_{\text{in}}\rangle \rightarrow |\psi_{\text{out}}\rangle$

$$\begin{aligned} |\psi_{\text{out}}\rangle &= \left(t\hat{a}_c^\dagger + ir\hat{a}_d^\dagger\right)\left(ir\hat{a}_c^\dagger + t\hat{a}_d^\dagger\right)|00\rangle_{c,d} \\ &= \left(irt\left(\hat{a}_c^\dagger\right)^2 + t^2\hat{a}_c^\dagger\hat{a}_d^\dagger - r^2\hat{a}_c^\dagger\hat{a}_d^\dagger + irt\left(\hat{a}_d^\dagger\right)^2\right)|00\rangle_{c,d} \end{aligned}$$

With this general HOM interference equation we consider a 50:50 beam splitter. This is the case where the HOM interference effect is most evident. Here, $r = t = 1/\sqrt{2}$, so the $\hat{a}_c^\dagger\hat{a}_d^\dagger$ terms cancel out, leaving

$$\begin{aligned} |\psi_{\text{out}}\rangle &= \frac{i}{2}\left(\hat{a}_c^\dagger\right)^2|00\rangle_{c,d} + \frac{i}{2}\left(\hat{a}_d^\dagger\right)^2|00\rangle_{c,d} \\ &= \frac{i}{2}|20\rangle_{c,d} + \frac{i}{2}|02\rangle_{c,d} \end{aligned}$$

which means that the two photons always bunch together, and the coincidence output state $|11\rangle_{c,d}$ will never occur. This remarkable result depends on the π phase difference in quantum amplitudes of the photon pair; a quan-

tum mechanical property that has no classical equivalent.

Note that in this derivation the assumption has been made that the outgoing photons produced from one incoming beam are indistinguishable to those produced from the other incoming beam. The positions, directions, polarisations, spatial modes, etc, of photons are the same at and after the beam splitter. In other words, the photons needs to be in identical modes in every degree of freedom. Since the creation operators correspond to a single mode they only completely cancel if both photons are described by a single $\hat{a}^\dagger$. If this is not the case, the creation operators for coincidence counts do not cancel out. Any error in mode matching exhibits as imperfect interference [16].

It is also interesting to note that as the beam splitter ratio changes from 50:50 by a small amount, the amplitude of the $|11\rangle_{c,d}$ state, and thus the likelihood of measuring a coincidence, increases. The changing beam splitter ratio introduces a statistical distinguishability since the photons in one output beam become more likely to have originated in a particular input beam.

How "good" a HOM interference dip is in practise is quantified by its *visibility*. The visibility V of a HOM dip is usually quoted as a percentage, and is defined as[2]

$$V = \frac{C_{\max} - C_{\min}}{C_{\max}}$$

where $C_{\max}$ is the coincidence rate outside the interference region, and $C_{\min}$ is the minimum coincidence rate when HOM interference is observed. The ideal HOM dip of a 50:50 beam splitter shown in Figure 3.1 has 100% visibility. Experimentally, the visibility of the dip depends on the distinguishability of the coincident photons. 90% visibility is typically achievable.

3.2 The CNOT Circuit

The layout of the circuit is shown in Figure 3.3. The circuit implements a CSIGN gate which, with the addition of half-wave plates implementing the Hadamard gates on the target before and after (see Section 2.3), is equivalent to a CNOT gate. [7, 17]

[2]Note that this definition of visibility for HOM interference, which is in standard use, is different from the definition of visibility for classical interference.

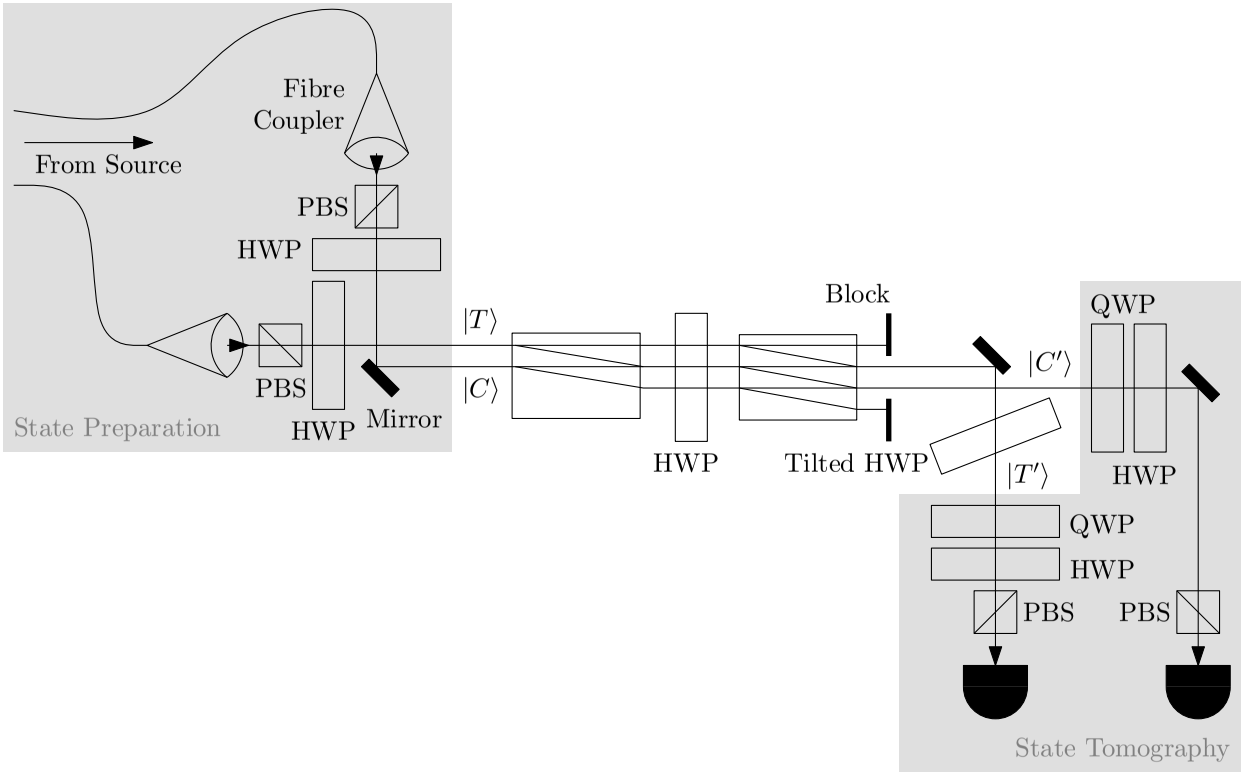

Figure 3.3: The layout of the optical CNOT circuit. Shaded regions represent preparation and tomography. The unshaded region constitutes a CSIGN gate. The CNOT gate is achieved by logically incorporating the required Hadamard gates on the target qubit into the preparation and tomography stages. The CSIGN generates a sign change due to HOM interference in the middle mode between the HWP and the second beam displacer.

The circuit works by changing the encoding of input qubits from polarisation to spatial encoding via a polarising beam displacer [18], a piece of birefringent material cut to displace or "walk-off" one polarisation with respect to another. In reference to Figure 3.3, the horizontal polarisation components of photons are displaced down, in our experiment by a distance of 4 mm, while vertical polarisation components of photons travel undeviated.

Beam displacers have a number of advantages over beam splitters. The main advantage is insensitivity to common-mode x, y, z translation noise. Rotations about the vertical axis are not common mode, however experimental evidence suggests that such rotations are not a problem — visibilities of classical interferometers using beam displacers of up to 97% have been measured.

The control and target input beams are separated by 4 mm in the beam displacer, ensuring that the displaced H (representing $|0\rangle$, say) of one input travels in the same space as the straight-through V (representing $|1\rangle$, say) of the other input. The HWP between the first and second beam displacers is set at an angle (17.6° from the optic axis) such that, when combined with the beam displacer after it, its operation is like that of a 1/3 beam splitter — the required condition for a CSIGN.

We see what the circuit does for logical control input states, $|0\rangle$ and $|1\rangle$. For a control input of $|0\rangle$ we expect there to be no effect on the target. Indeed this is the case. The control photon is displaced out of the paths of the target photon. The target photon travels through the interferometer, is recombined by classical interference and then examined in the tomography region of the circuit. The beam displacers are aligned so that the interferometer is balanced and the output is found in the same polarisation as the input.

For a control input of $|1\rangle$, however, we expect there to be a sign change on the $|1\rangle$ portion of the input. The $|0\rangle$ portion of the target input travels along the top path and does not interact with the control. The $|1\rangle$ portion, on the other hand, is displaced down into the path of the control photon. The HWP causes the polarisations to rotate to a partially indistinguishable state (in the H/V basis as discriminated by the beam displacer).

It is this indistinguishability that causes HOM interference on the surface of the beam displacer. Since the HWP acts as a 1/3 beam splitter, and not a 50:50 beam splitter, the HOM interference has an ideal visibility of 80%.

The circuit detection considers only coincident photons, which requires the two photons in the interfering beam to seperate. Since the HOM interference only has 80% visibility this occurs 1/9 of the time.

By replacing r and t in the general equation for HOM interference derived earlier, we see what happens to our target photon. For a 1/3 beam splitter, $r = 1/\sqrt{3}$ and $t = \sqrt{2/3}$, so the equation for HOM interference becomes

$$|\psi_{\text{out}}\rangle = \left(i\frac{\sqrt{2}}{3}\left(\hat{a}_c^\dagger\right)^2 + \frac{2}{3}\hat{a}_c^\dagger\hat{a}_d^\dagger - \frac{1}{3}\hat{a}_c^\dagger\hat{a}_d^\dagger + i\frac{\sqrt{2}}{3}\left(\hat{a}_d^\dagger\right)^2 \right)|00\rangle_{c,d}$$

The $\left(\hat{a}^\dagger\right)^2$ terms can be ignored since they do not contribute coincidence counts. The two other modes have picked up a relative sign difference by the interference that did not exist in the original beams. By recombining the two spatially separated modes via the second beam displacer the negative sign propagates, and so the circuit works as expected.

The central HWP has two important effects other than allowing the HOM interference to occur. Firstly, it causes the roles of H and V to swap. This allows the same type of beam displacer to be used to recombine the spatial encoding of each qubit back into polarisation encoding, but it also means that the interpretation of H as $|0\rangle$ and V as $|1\rangle$ has changed after the gate. This effect can easily be corrected, either by addition of a HWP at 45° from its optic axis to flip H and V, or logically when performing analysis. Secondly, the HWP is applied equally to each spatial mode, which ensures that as the photons then pass through the beam displacer, all probabilities are balanced.

The circuit requires two balanced classical interferometers. We balance one interferometer by moving and rotating the beam displacers. Doing this, however, removes any remaining degrees of freedom to balance the second interferometer. This is why we include a HWP in the other output arm, before the analysis components, set at its optic axis but tilted around the vertical axis in such a way as to balance the interferometer. The birefringence of the HWP at this tilt corrects for any remaining phase difference in H and V.

The results of operation of this circuit will be presented in Chapter 6.

3.3 Weak Measurements Of Photons

As demonstrated by Pryde et al [8], weak measurements can be performed on photons using the CNOT as a QND device. By using polarisation states between H and D (diagonal polarisation, 45° from H and equal to $\frac{1}{2}(|H\rangle + |V\rangle)$) for the meter input we can achieve the weak measurement condition exactly as described in Section 2.5.

By setting the meter to some intermediate polarisation we obtain partial information about the signal. Say the meter state is $|M\rangle = \alpha|H\rangle + \beta|V\rangle$. Different values of α and β give us different contributions to the resulting polarisation from the amplitudes of the signal. A value of α larger than β would mean more contribution of the signal's H to the resulting meter output's H polarisation and less to V, and the opposite for the signal's V, meaning that we could be more sure about the result being an accurate representation of the signal state.

Interestingly, measuring the meter output puts the signal output in a partly mixed state [8]. The degree of mixture depends on how much correlation there is between the meter output and the signal input as the meter is measured.

Chapter 4

Unambiguous State Discrimination

4.1 Ambiguous States

Imagine a measurement on an unknown system to discriminate between two orthogonal states. We can think of this as performing a 'yes'/'no' test on the system to see if it is in one particular state of the two. When a successful result is found we know for certain that the system was in that state, and when a 'no' is found, we know for certain that the system must have been in the other state. In principle, distinguishing orthogonal states in quantum mechanics can always be done with a single-shot measurement [2].

When trying to differentiate between two *non*-orthogonal states it becomes impossible to be so sure about which state is which. Consider a pair of non-orthogonal basis states $|\psi_+\rangle = \cos\theta\,|0\rangle + \sin\theta\,|1\rangle$ and $|\psi_-\rangle = \cos\theta\,|0\rangle - \sin\theta\,|1\rangle$ centered around $|0\rangle$ as in Figure 4.1. Because these states are not orthogonal, their inner product $\langle\psi_+|\psi_-\rangle$ is non-zero.

Suppose we have the state $|\phi\rangle = |\psi_\pm\rangle$, i.e. either $|\psi_+\rangle$ or $|\psi_-\rangle$, and we wish to determine which via a measurement. If we were to perform a projective measurement on $|\phi\rangle$ we might first try the projection onto $|\psi_+\rangle$. The probability of a successful result would depend on the overlap of the basis and the unknown states, namely $P = |\langle\psi_+|\phi\rangle|^2$.

Now suppose that $|\phi\rangle$ is actually in the $|\psi_-\rangle$ state. This probability of projection would reduce to $P = |\langle\psi_+|\psi_-\rangle|^2$. This is not zero, so there is some probability that a measurement against $|\psi_+\rangle$ will be successful *even*

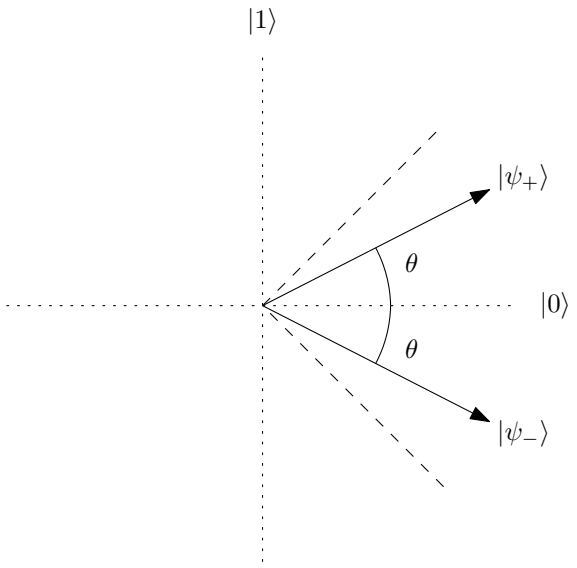

Figure 4.1: An example of nonorthogonal states. The dotted lines are orthogonal to each other, and $\theta < \pi/4$ radians. Discriminating between two nonorthogonal states presents problems since a system in one state might collapse onto the other state.

if the state being measured was prepared in the $|\psi_-\rangle$ state. Figure 4.2 shows the relationship between the orthogonality of the two states and the likelihood that a system in one state will be measured as being in the other state.

Nielsen and Chuang prove [2, pg. 87] that nonorthogonal states can never be reliably distinguished. There will always be an amount of error proportional to the overlap of the two basis states. By choosing the measurement bases carefully, this error can be decreased to the Helstrom limit [19]

$$P_{\text{Error}} = \frac{1}{2}\left(1 - \sin 2\theta\right)$$

This is the lowest error possible by using standard projective measurements, and is achieved by projecting onto the nearest pair of orthogonal states. The dotted lines in Figure 4.1 are an example of such states, and projecting onto these is known as a Helstrom measurement [19].

Figure 4.2: Probability of erroneously discriminating a nonorthogonal state using a projective measurement in the Helstrom limit. This is the smallest possible likelihood of error in discrimination. For nearly identical states, the probability of error approaches $1/2$. As the separation between states increases towards orthogonality, the probability of erroneous discrimination goes to zero.

4.2 The Mechanism Of USD

The idea of *Unambiguous State Discrimination* (USD), first described by Ivanovic [20], is that the error due to discrimination of states by projection can be isolated in a third inconclusive, or 'don't know', result. We denote this as a measurement resulting in the $|\psi_?\rangle$ state. It can be shown that nonorthogonal states can be discriminated with complete accuracy, with the caveat that sometimes a result of $|\psi_?\rangle$ will be obtained and nothing can be said about the state of a system being measured.

We implement this by considering two projective measurements on the unknown $|\phi\rangle$ against states *orthogonal* to each of the basis states $|\psi_+\rangle$ and $|\psi_-\rangle$, as in Figure 4.3. If a successful measurement is made onto $|\overline{\psi}_+\rangle$, the orthogonal state to $|\psi_+\rangle$, we can be sure that $|\phi\rangle$ was not in the state $|\psi_+\rangle$, and so it must have been in the state $|\psi_-\rangle$. If, however, the measurement is not successful, this could be due to one of two reasons, namely that

1. the state was really $|\psi_+\rangle$, or

2. the $|\psi_-\rangle$ state did not collapse onto the measured state $|\overline{\psi}_+\rangle$.

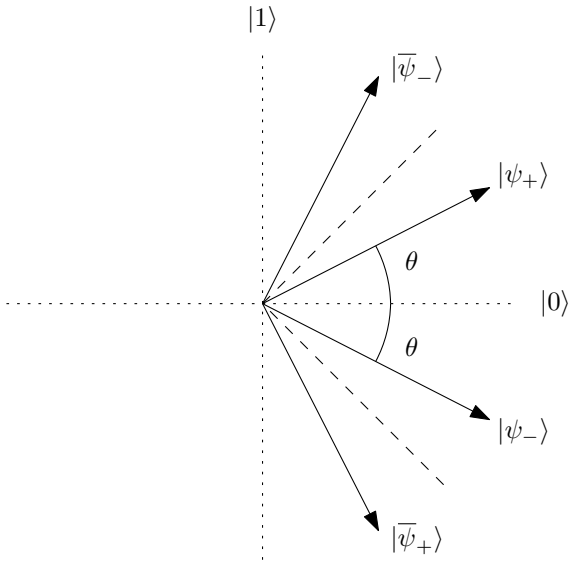

Figure 4.3: Nonorthogonal states and their orthogonal counterparts. $|\overline{\psi}_+\rangle$ is orthogonal to $|\psi_+\rangle$, $|\overline{\psi}_-\rangle$ is orthogonal to $|\psi_-\rangle$, and the dotted lines are orthogonal to each other.

The only way to know which is true is to simultaneously perform a projective measurement of $|\phi\rangle$ onto $|\overline{\psi}_-\rangle$. If this measurement is a success, then we know for certain that $|\phi\rangle = |\psi_+\rangle$, and if not, we know nothing about $|\phi\rangle$.

Unambiguous state discrimination is a *Positive Operator Value Measurement* (POVM) that can be thought of as the triplet of measurements, represented by the operators $\hat{M}_+$, $\hat{M}_-$ and $\hat{M}_?$. $\hat{M}_+$ is the measurement against $|\overline{\psi}_-\rangle$, and $\hat{M}_-$ is the measurement against $|\overline{\psi}_+\rangle$. $\hat{M}_?$ is the remaining measurement in the POVM, found by the POVM property $\sum_i \hat{E}_i = \hat{\mathbb{1}}$, where $\hat{E}_i \equiv \hat{M}_i^\dagger \hat{M}_i$ are the POVM elements.

With these parameters one can build the entire POVM operator set starting with

$$\begin{aligned} \hat{E}_+ &= c\,|\overline{\psi}_-\rangle\langle\overline{\psi}_-| \\ \hat{E}_- &= c\,|\overline{\psi}_+\rangle\langle\overline{\psi}_+| \\ \hat{E}_? &= \hat{\mathbb{1}} - \hat{M}_+ - \hat{M}_- \end{aligned}$$

for some constant c. By only considering states where $\theta < \pi/4$ and using the fact that $\hat{E}$ are represented by Hermitian matrices, we find the optimum measurement $c = \left(2\cos^2\theta\right)^{-1}$ and the POVM elements in the $|0\rangle/|1\rangle$ basis

are

$$\begin{aligned}
\hat{E}_+ &= \frac{1}{2}\begin{bmatrix} \tan^2\theta & \tan\theta \\ \tan\theta & 1 \end{bmatrix} \\
\hat{E}_- &= \frac{1}{2}\begin{bmatrix} \tan^2\theta & -\tan\theta \\ -\tan\theta & 1 \end{bmatrix} \\
\hat{E}_? &= \begin{bmatrix} 1-\tan^2\theta & 0 \\ 0 & 0 \end{bmatrix}
\end{aligned}$$

4.3 Three Results From A Two-Basis System

Consider an unknown state we wish to distinguish unambiguously, $|\phi\rangle = |\psi_\pm\rangle$. The probability of a successful measurement with an element $\hat{E}_\pm$ should correspond to the state sent in. The probability for $\hat{E}_+$ is

$$\left\langle \psi_\pm \middle| \hat{E}_+ \middle| \psi_\pm \right\rangle = \frac{1}{2\cos^2\theta} \langle \psi_\pm | \overline{\psi}_- \rangle \langle \overline{\psi}_- | \psi_\pm \rangle$$

So for $|\psi_+\rangle$ states the probability is $\frac{1}{2\cos^2\theta}|\langle\psi_+|\overline{\psi}_-\rangle|^2 = 2\sin^2\theta$, and for $|\psi_-\rangle$ states the probability is 0.

Conversely for the $\hat{E}_-$ element, the probability for $|\psi_+\rangle$ states is 0 and the probability for $|\psi_-\rangle$ states is $2\sin^2\theta$. This illustrates that $\hat{E}_+$ will only ever succeed on $|\psi_+\rangle$ states, but with some non-unit probability, and similarly $\hat{E}_-$ only on $|\psi_-\rangle$ states with non-unit probability.

The remaining probability can be found in the $\hat{E}_?$ element

$$\begin{aligned}
\left\langle \psi_\pm \middle| \hat{E}_? \middle| \psi_\pm \right\rangle &= \left(1-\tan^2\theta\right) \langle \psi_\pm | 0 \rangle \langle 0 | \psi_\pm \rangle \\
&= \left(1-\tan^2\theta\right)\cos^2\theta \\
&= \cos^2\theta - \sin^2\theta \\
&= \cos 2\theta
\end{aligned}$$

The third result of the USD triplet, $|\psi_?\rangle$, encompasses all the uncertainty inherent in discrimination of non-orthogonal states. What this means in practice is that all the uncertainty required by the fact that the basis states are non-orthogonal is channelled into this 'don't know' state. So any of the three results may be obtained for any one unambiguous measurement, however if we receive anything other than $|\psi_?\rangle$ for that measurement we

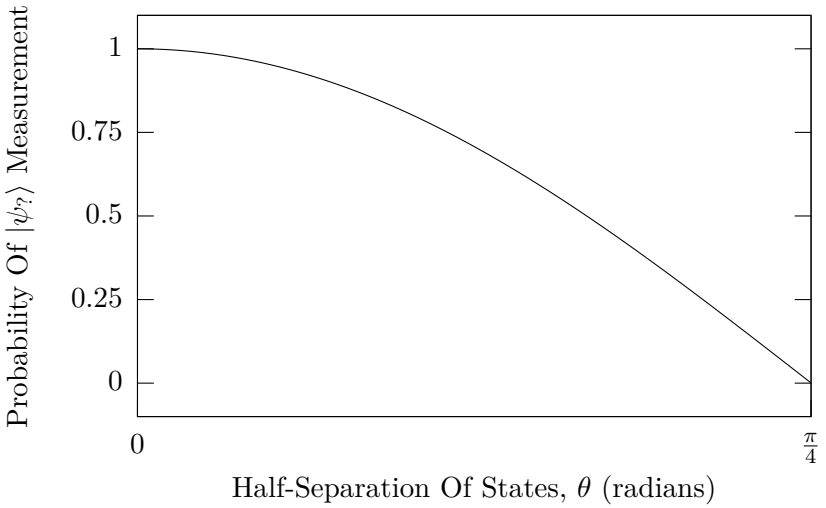

Figure 4.4: Probability of finding the inconclusive state $|\psi_?\rangle$ through a USD measurement. States that are almost identical will almost exclusively give the inconclusive result. As the separation between states increases towards orthogonality, the likelihood of an inconclusive result decreases to zero.

know for certain which state the unknown system was in. The probability of obtaining a conclusive measurement is simply $1 - \cos 2\theta = 1 - |\langle\psi_+|\psi_-\rangle|$ [21]. This is an optimal USD measurement in the sense that it has the smallest possible likelihood of obtaining the $|\psi_?\rangle$ result.

4.4 USD On Entangled States

We plan to explore the use of the CNOT to produce QND entangled signal and meter qubits, performing an unambiguous state discrimination measurement on the meter. Since doing so produces entanglement in the system during the protocol we shall analyse the effect of performing USD on an entangled state.

Consider the signal input state $|S\rangle = |\psi_\pm\rangle = \cos\theta\,|0\rangle \pm \sin\theta\,|1\rangle$, and the meter state $|M\rangle = |0\rangle$ as for a QND measurement. The entangled state resulting from the CNOT operation is $|S'M'\rangle = \cos\theta\,|00\rangle \pm \sin\theta\,|11\rangle$. To fully analyse the evolution of states we turn to density matrix form. As a

density matrix $\hat{\rho}$, $|S'M'\rangle$ is

$$\hat{\rho} = \begin{bmatrix} \cos^2\theta & 0 & 0 & \pm\cos\theta\sin\theta \\ 0 & 0 & 0 & 0 \\ 0 & 0 & 0 & 0 \\ \pm\cos\theta\sin\theta & 0 & 0 & \sin^2\theta \end{bmatrix}$$

To find the probability of getting the $\hat{E}_+$ measurement of the meter, representing the $|\psi_+\rangle$ state, we take the trace of the result of applying $\hat{E}_+^M \equiv \hat{\mathbb{1}} \otimes \hat{E}_+$ to $\hat{\rho}$.

$$\begin{aligned} & P\left(\hat{E}_+^M \mid \hat{\rho}\right) = \mathrm{Tr}\left(\hat{E}_+^M \hat{\rho}\right) \\ & = \frac{1}{2}\mathrm{Tr}\left(\begin{bmatrix} \tan^2\theta & \tan\theta & 0 & 0 \\ \tan\theta & 1 & 0 & 0 \\ 0 & 0 & \tan^2\theta & \tan\theta \\ 0 & 0 & \tan\theta & 1 \end{bmatrix} \begin{bmatrix} \cos^2\theta & 0 & 0 & \pm\cos\theta\sin\theta \\ 0 & 0 & 0 & 0 \\ 0 & 0 & 0 & 0 \\ \pm\cos\theta\sin\theta & 0 & 0 & \sin^2\theta \end{bmatrix}\right) \\ & = \frac{1}{2}\mathrm{Tr}\left(\begin{bmatrix} \sin^2\theta & 0 & 0 & \pm\sin^2\theta\tan\theta \\ \cos\theta\sin\theta & 0 & 0 & \pm\sin^2\theta \\ \pm\sin^2\theta & 0 & 0 & \sin^2\theta\tan\theta \\ \pm\cos\theta\sin\theta & 0 & 0 & \sin^2\theta \end{bmatrix}\right) \\ & = \sin^2\theta \end{aligned}$$

This has no dependence on whether the input was $|\psi_+\rangle$ or $|\psi_-\rangle$! Compare the operator for the $|\psi_-\rangle$ state, $\hat{E}_-$:

$$\begin{aligned} & P\left(\hat{E}_-^M \mid \hat{\rho}\right) = \mathrm{Tr}\left(\hat{E}_-^M \hat{\rho}\right) \\ & = \frac{1}{2}\mathrm{Tr}\left(\begin{bmatrix} \tan^2\theta & -\tan\theta & 0 & 0 \\ -\tan\theta & 1 & 0 & 0 \\ 0 & 0 & \tan^2\theta & -\tan\theta \\ 0 & 0 & -\tan\theta & 1 \end{bmatrix} \begin{bmatrix} \cos^2\theta & 0 & 0 & \pm\cos\theta\sin\theta \\ 0 & 0 & 0 & 0 \\ 0 & 0 & 0 & 0 \\ \pm\cos\theta\sin\theta & 0 & 0 & \sin^2\theta \end{bmatrix}\right) \\ & = \frac{1}{2}\mathrm{Tr}\left(\begin{bmatrix} \sin^2\theta & 0 & 0 & \pm\sin^2\theta\tan\theta \\ -\cos\theta\sin\theta & 0 & 0 & \mp\sin^2\theta \\ \mp\sin^2\theta & 0 & 0 & -\sin^2\theta\tan\theta \\ \pm\cos\theta\sin\theta & 0 & 0 & \sin^2\theta \end{bmatrix}\right) \\ & = \sin^2\theta \end{aligned}$$

The probability of each determinant measurement is the same regardless of which state was sent in[1]! It appears that naïvely plugging the two circuits together doesn't give us anything useful, but this is not the case[2].

To examine the states after the POVM measurement we need to know what $\hat{M}_+$, $\hat{M}_-$, and $\hat{M}_?$ are. Since $\hat{E}_i \equiv \hat{M}_i^\dagger \hat{M}_i$, we can represent the measurement operators as[3]

$$\begin{aligned}
\hat{M}_+ &= \frac{1}{\sqrt{2}} \begin{bmatrix} 0 & 0 \\ \tan\theta & 1 \end{bmatrix} \\
\hat{M}_- &= \frac{1}{\sqrt{2}} \begin{bmatrix} 0 & 0 \\ -\tan\theta & 1 \end{bmatrix} \\
\hat{M}_? &= \begin{bmatrix} \sqrt{1-\tan^2\theta} & 0 \\ 0 & 0 \end{bmatrix}
\end{aligned}$$

Applying $\hat{M}_+^M \equiv \hat{\mathbb{1}} \otimes \hat{M}_+$ to the signal/meter system $\hat{\rho}$ and normalising gives

$$\frac{\hat{M}_+^{M\dagger} \hat{\rho} \hat{M}_+^M}{P\left(\hat{E}_+^M \mid \hat{\rho}\right)} = \frac{1}{2} \begin{bmatrix} 0 & 0 & 0 & 0 \\ 0 & 1 & 0 & \pm 1 \\ 0 & 0 & 0 & 0 \\ 0 & \pm 1 & 0 & 1 \end{bmatrix}$$

This is the state we would have after a successful measurement in $|\psi_+\rangle$, though we can't be sure that this was the actual state of the signal. We can already see, though, that by examining the S' state we might be able to obtain information about whether the successful measurement was true or false.

We take the partial trace over M' to find

$$\hat{\rho}_{S'} = \frac{1}{2} \begin{bmatrix} 1 & \pm 1 \\ \pm 1 & 1 \end{bmatrix}$$

Evidently the signal has been orthogonalised by the QND back-action from

[1] Credits to Ben Lanyon, who discovered this alarming result in the middle of construction of the experiment.

[2] Credits to Geoff Pryde for discovering the solution.

[3] Actually, the result of any single-qubit unitary operation on these $\hat{M}_i$'s is a sufficient representation of the measurement operators. Without loss of generality we consider only these cases.

the USD operation on the meter[4]. If we were to measure S' in the $|+\rangle = \frac{1}{\sqrt{2}}(|0\rangle + |1\rangle)$ and $|-\rangle = \frac{1}{\sqrt{2}}(|0\rangle - |1\rangle)$ basis, we would find the probability of obtaining $|+\rangle$ is 1 and $|-\rangle$ is 0 for $|\psi_+\rangle$ states, but for $|\psi_-\rangle$ states the probability of obtaining $|-\rangle$ is 1 and $|+\rangle$ is 0.

What this means is that a measurement of S' in the $|+\rangle/|-\rangle$ basis will tell us if the $|\psi_+\rangle$ result in T' was true. If S' is $|+\rangle$, then the measurement was true and T' is $|\psi_+\rangle$, but if S' is $|-\rangle$, the measurement was false and T' is $|\psi_-\rangle$.

Let us also consider $\hat{M}_-^M$. The system after this measurement is successful is in the state

$$\frac{\hat{M}_-^{M\dagger}\hat{\rho}\hat{M}_-^M}{P\left(\hat{E}_-^M \mid \hat{\rho}\right)} = \frac{1}{2}\begin{bmatrix} 0 & 0 & 0 & 0 \\ 0 & 1 & 0 & \mp 1 \\ 0 & 0 & 0 & 0 \\ 0 & \mp 1 & 0 & 1 \end{bmatrix}$$

By taking the partial trace over M' we have

$$\hat{\rho}_{S'} = \frac{1}{2}\begin{bmatrix} 1 & \mp 1 \\ \mp 1 & 1 \end{bmatrix}$$

and by measuring S' in the $|+\rangle/|-\rangle$ basis, we find the probability of obtaining $|+\rangle$ is 0 and $|-\rangle$ is 1 for $|\psi_+\rangle$ states, and $|-\rangle$ is 0 and $|+\rangle$ is 1 for $|\psi_-\rangle$ states.

This shows that the measurement on the signal tells us the truth or falsehood of the USD measurement on the meter. A result of $|+\rangle$ in the signal tells us that the meter measurement is correct, while a result of $|-\rangle$ in the signal tells us that the meter measurement is false and that the signal was originally in the other state.

For completeness we also consider the effect on S' of the 'don't know' measurement $\hat{M}_?^M$. We find

$$\frac{\hat{M}_?^{M\dagger}\hat{\rho}\hat{M}_?^M}{P\left(\hat{E}_?^M \mid \hat{\rho}\right)} = \frac{1}{2}\begin{bmatrix} 1 & 0 & 0 & 0 \\ 0 & 0 & 0 & 0 \\ 0 & 0 & 0 & 0 \\ 0 & 0 & 0 & 0 \end{bmatrix}$$

[4]The state $\frac{1}{2}\begin{bmatrix} 1 & 1 \\ 1 & 1 \end{bmatrix}$ is orthogonal to $\frac{1}{2}\begin{bmatrix} 1 & -1 \\ -1 & 1 \end{bmatrix}$.

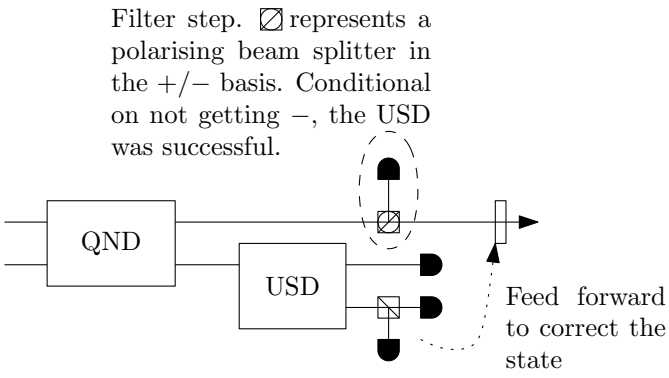

Figure 4.5: A USD success filter. USD on entangled states results in a signal state in one of two orthogonal states that directly correspond to the truth or falsehood of the conclusive result of the meter. By using a beam splitter set to reflect polarisations that indicate a false result into a detector, whenever such a state is not detected, the discrimination must have been a true success.

Thus, for $|\psi_?\rangle$ states, the signal qubit will always be found at $|0\rangle$.

What all this means in practice is that we need some sort of discrimination method on the signal output to be able to determine true results. We do this by filtering the signal output on $|+\rangle/|-\rangle$. By adding detection of $|-\rangle$ states we can remove all the incorrect results from the stream of qubits (see Figure 4.5). This means that half of the results are removed, but the successful results have been obtained non-destructively — conditional on not achieving the $|-\rangle$ outcome.

In order to perform this state discrimination with 100% success a second QND or QND-like operation would need to be performed on the signal to determine which orthogonal state it was in after the non-destructive USD.

Finally, to ensure that the final state of the signal qubit is not identical in both the $|\psi_+\rangle$ and $|\psi_-\rangle$ cases, we would need to rotate $|S'\rangle$ dependent on the measurement outcome. This can be done in principle using feed-forward techniques [22, 23], but for simplicity we will omit this step here.

At this point, it should be emphasised again that what we are attempting with this project is an exploration of what can be achieved in terms of generalised measurements, and in particular, non-destructive generalised measurements. As such, we are not proposing that the approaches described would necessarily be more effective than, say, an eavesdropper using a "detect and re-prepare" strategy in quantum key distribution.

It is interesting to note that, without the filter or second QND step the circuit acts as a controlled non-unitary gate. The gate can generate maximally-entangled states from non-orthogonal states, and it turns out that by changing the state of the target input to the CNOT part of the circuit the degree of entanglement generated by the operation can be controlled. This gate works because of the fact that the USD measurement distills a maximally entangled state from a non-maximally entangled state.

4.5 Imperfectly Mode-Matched CNOT States And USD

Accurate mode matching is very important for the operation of the optical CNOT gate [13, 24]. Without perfectly overlapped beams the HOM interference does not work at optimum capability and the gate operation degrades. This degradation occurs for control inputs of $|1\rangle$, since they employ the HOM interference, however $|0\rangle$ control states operate as well as for perfectly overlapped beams.

This asymmetry in operation when imperfection is introduced to the HOM interference complicates the effect of the USD device. It turns out that the imperfect HOM interference and USD on the entangled target output qubit exaggerates mixture in the state of the control output qubit [25]. Since achieving a HOM interference of visibility greater than 90% is extremely difficult without specialised components, we expect to see that this mixture is evident in our state measurements.

Chapter 5

Optical Realisation Of USD

An optimal implementation of unambiguous discrimination of non-orthogonal polarisation states of photons has been demonstrated previously [6, 9]. We use a simplified instance of the circuit used by Clarke et al [9] and replace the interferometer polarising beam splitters with polarising beam displacers, for the same reasons they were used in the realisation of the CNOT gate, and for consistency. This implements the optimum case of the USD POVM described in Section 4.2.

5.1 Operation Of Optical USD

The circuit attempts to orthogonalise non-orthogonal input states by diverting some of the common polarisation component into an extra mode. The circuit discriminates states probabilistically, with success conditional on not detecting a photon in this extra mode. We start with one of two orthogonal states centered around a common polarisation state, in the experiment by Clarke et al and this example, horizontal polarisation, H. The actual base used is unimportant, but for consistency we demonstrate the operation based around H. (Our experiment performs the same operations around the vertical polarisation V.)

The effect of the circuit on input states is illustrated by Figures 5.2–5.5. The circuit separates the input (1) into its vertical (2) and horizontal (3) components (Figure 5.2). We can already see that the only difference between the two states is the direction of the vertical component, representing its phase with respect to the horizontal component.

To orthogonalise the state we want to make the size of the horizontal component equal the size of the vertical component. To do this, the horizontal part (3) is rotated (4) (Figure 5.3). When this new state is separated into its H and V components (Figure 5.4) the horizontal component (6) has the same magnitude as the original vertical component (2). The new vertical component (5) represents the $|\psi_?\rangle$ state.

Finally, the equal horizontal (6) and vertical (2) components are recombined (Figure 5.5), and the resulting orthogonal state (7) can be discriminated with a standard projective measurement in the diagonal basis, i.e. against diagonal (D, 45° from H) and anti-diagonal (A, −45° from H) polarisations.

Any one qubit will be detected either at the D/A discriminating detector or at the $|\psi_?\rangle$ state detector, which receives the vertical component (5) resulting from rotation of the horizontal component of the input. The likelihood that the unknown state will be detected depends on the magnitude of the vertical component (5), which is determined by the amount of rotation performed in Step 2. This rotation must be set so that the magnitude of the horizontal component that is left is the same as the magnitude of the original input's vertical component, and so it will be different for each pair of possible non-orthogonal states. For nearly orthogonal input states, there will be minimal extra horizontal component, which needs to be rotated minimally, and thus will have only a small vertical component (5).

5.2 The USD Circuit

The detailed layout of the circuit used is shown in Figure 5.1 on the following page. This circuit discriminates states around V, though it could be made to work on states around H with the addition of a HWP to flip the input.

A polarising beam displacer splits the H and V components of the input, separating the beams by 4 mm. A HWP flips the horizontal of the first arm to vertical, while another HWP beside it flips and rotates the vertical in the second arm such that its remaining horizontal component is equal in magnitude to the vertical in the first arm. This requires the waveplate to be at an angle of $\arccos\tan\theta$ plus its optic axis. Since the two beams are separated by only 4 mm, these two HWPs are unmounted, and are held in place in the circuit by claws. This makes precise adjustments very difficult

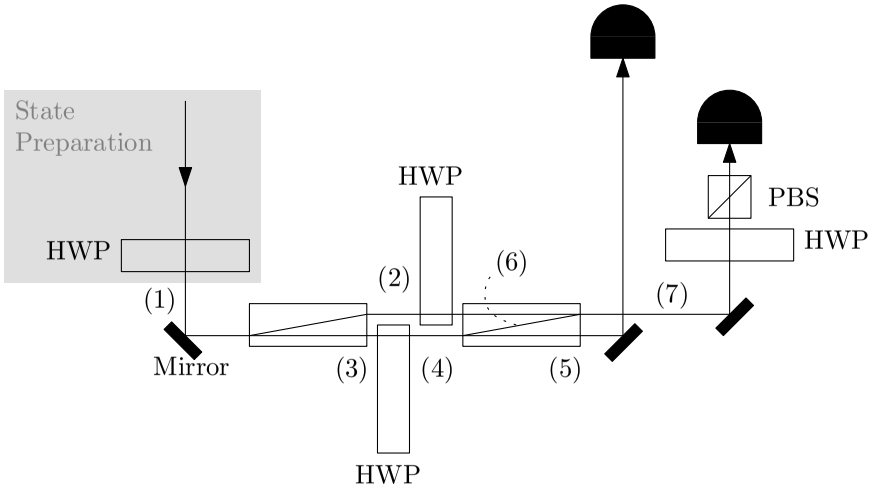

Figure 5.1: Layout of the optical USD circuit. The input system arrives from state preparation and is split by the first beam displacer. The two central half-wave plates rotate the polarisations so that, when recombined by the second beam displacer, the components of each polarisation are equal. This state can then be discriminated by an orthogonal measurement. The difference in polarisation is left in another mode, and heralds the inconclusive result. The numbers (1)–(7) refer to states in Figures 5.2–5.5.

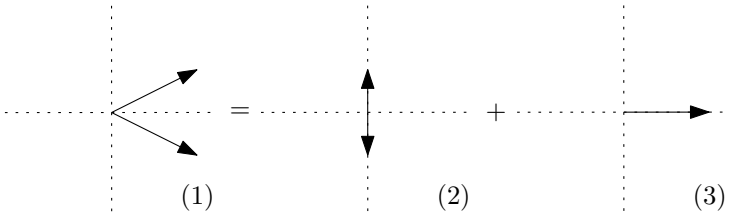

Figure 5.2: Operation of the USD, step 1. The input state is separated into vertical and horizontal components.

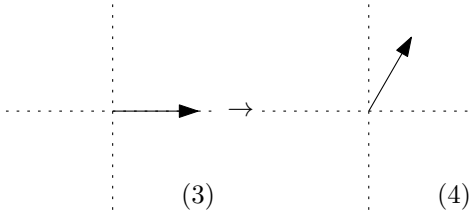

Figure 5.3: Operation of the USD, step 2. The horizontal component is rotated so that the remaining horizontal component has the same magnitude as the vertical component that was separated off in Step 1.

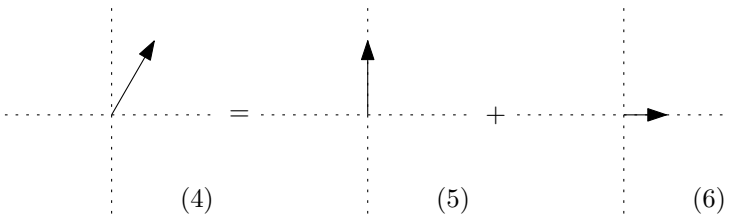

Figure 5.4: Operation of the USD, step 3. The new state is then separated into its own vertical and horizontal components. The remaining vertical component represents the $|\psi_?\rangle$ state.

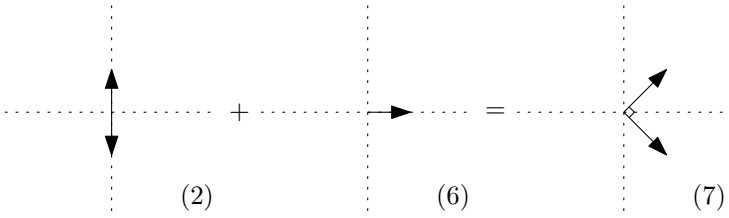

Figure 5.5: Operation of the USD, step 4. The remaining horizontal component from Step 3 is recombined with the vertical component from Step 1. The resulting state can then be discriminated by a projective measurement.

as they have to be rotated in place by hand[1].

The vertical components pass through the second polarising beam displacer, and the horizontal component recombines with the vertical component of the input, leaving D or A (depending on the input) which are discriminated at a polarisation analyser. A detection of D signals a discrimination of the $|\psi_+\rangle$ state, while a detection of A signals a discrimination of the $|\psi_-\rangle$ state. The remaining vertical component is directed to another detector. If the photon collapses into this mode it signals the inconclusive result, $|\psi_?\rangle$.

This USD circuit was constructed and tested, the results presented in Chapter 6.

[1] Or more precisely: by finger.

Chapter 6

Combining QND And USD — The Experiment

We aim to explore the issues surround extensions of general measurements in quantum mechanics. To do this we combine a quantum non-demolition measurement device with an unambiguous state discrimination device in an attempt to devise a non-demolition unambiguous discriminator of non-orthogonal states.

This chapter details the experiment and its results. We present the source setup and properties of the light used in the experiment. We also cover the criterion of detection of coincident photons. The results of finding the Hong-Ou-Mandel interference dip, and using the CNOT on logical states and states that produce maximal entanglement are also presented. We then cover the results of USD analysis on states 22.5° from V. Finally, the density matrices of the states resulting from the combined operation of the CNOT as a QND device and the USD device are presented and characterised for both the strong and weak measurement cases.

The CNOT gate and USD circuit described in previous sections are constructed sequentially so that an output of the CNOT becomes the input of the USD device. The combination of the two devices gives a grand total of 4 interference phenomena and 18 calibrated common-mode polarisation components. A schematic of the experiment can be seen in Figure 6.1.

The CNOT circuit described in Section 3.2 operates on the basis that H represents $|0\rangle$ and V represents $|1\rangle$. For the combination of QND and USD in this experiment it was logistically convenient that the target and

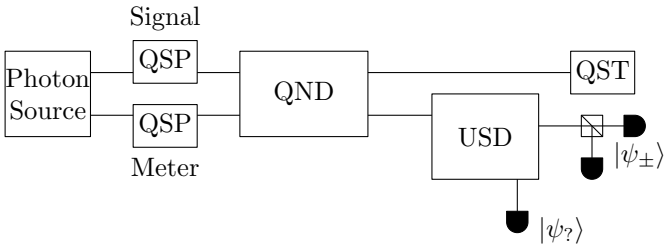

Figure 6.1: Schematic of the experiment. The source produces photons which undergo quantum state preparation (QSP) and are then entangled by the QND device. The meter photon then undergoes unambiguous state discrimination (USD), and quantum state tomography (QST) is performed on the signal photon. The lower detector attached to the output of the USD device detects inconclusive results, while the two detectors at the side detect conclusive results of $|\psi_+\rangle$ and $|\psi_-\rangle$.

control inputs were swapped, requiring a change of the basis states to $|0\rangle$ being represented by V, and $|1\rangle$ being represented by H. In either case the operation is identical (to within local unitaries) and the circuit works just as effectively. The remainder of the thesis assumes this representation.

6.1 The Photon Source

The experiment requires pairs of coincident photons — photons that travel through the quantum circuit at the same time so that they interfere with each other. These photons were generated using an existing spontaneous parametric down-conversion [26] source comprising a Titanium-Sapphire (Ti:Saph) mode-locked laser and frequency conversion crystals.

The Ti:Saph laser produces an 820 nm beam of light with typical average power output of 1.5 W and pulse lengths of $\sim$ 100 fs at 80 MHz repetition rate. This pumps a birefringent bismuth borate (BiB_3O_6 or BiBO) crystal cut for collinear 2nd harmonic generation, giving 700 μW of light at 410 nm. This in turn pumps a down-converter crystal[1] which produces pairs of coincident photons through a type I spontaneous parametric down-conversion (SPDC) process [14].

[1] We in-fact used the second pass of a two-pass down-conversion setup. The 410 nm pump beam passed through the down-conversion crystal once where coincident pairs were extracted and taken to another experiment. The remainder of the pump beam then hit a retroreflecting mirror, and passed through the down-conversion crystal in the opposite direction, where coincident photons were extracted and taken to this experiment.

The SPDC process produces concentric cones of light. The wavelength of the photons on the surface of a cone are the same and are related to the cone's internal angle. Mirrors are placed at opposite sides of the 820 nm light cone, directing light beams which pass through wavelength filters and couple to single-mode optic fibres, ensuring that only photons with very nearly 820 nm wavelength are captured. In this way we collect degenerate coincident photons which are then guided to the inputs of our circuit by optic fibres. Single-mode optic fibres were used to maintain quality Gaussian shaped-beams necessary for HOM interference, and to ensure minimal loss between the source and the experiment.

Two down-conversion crystals were used at different stages of the experiment due to an unavoidable change in the source[2]. A β-barium borate (β-BaB_2O_4 or BBO) crystal cut for type I SPDC was used first. This crystal employs a non-linear process to convert a beam of 410 nm photons into pairs of noncollinear coincident photons in a process that conserves energy and momentum. The result is cones of photons whose energy determines the steepness of the cone it traverses. For an energy-degenerate pair of coincident photons, the cones which those photons occupy overlap completely. Two fibre couplers capture these degenerate photons. Roughly 30000 coincident pairs per second were able to be extracted using this mechanism.

Later, the BBO was replaced by a bismuth borate (BiB_3O_6 or BiBO) crystal cut for type I SPDC, which possesses the same functionality as the BBO but with higher efficiency due to a higher nonlinear coefficient [27]. It was found that 60000 coincident pairs were able to be extracted in the same manner, double that of the BBO. Due to the loss inherent in all the fibres and optical components in the experiment, rates at our detectors were considerably lower for both BiBO and BBO, in some cases by a factor of over 100.

Occasionally, the down-converting crystal produces a *four-fold* coincidence event where two pump photons enter the crystal at the same time and both are down-converted. This results in a group of four photons that are all coincident. When this enters the circuit it becomes possible that erroneous coincidences occur, when photons which are not from a single input pair and don't correspond to different inputs couple into different outputs.

[2]When the BBO source previously used was burned over time, it was replaced with BiBO, which has a higher nonlinear coefficient.

These are detected as successful coincidences, but the pairs come from only one input and so the circuit could not possibly have performed successfully.

To account for the four-fold error, counts are taken with the circuit in the same configuration as for regular data taking, except that one of the two inputs are blocked. The same is done for the other input, and the addition of these two values gives an estimate of the rate of four-folds that contribute to a measurement in that configuration. Typical total rates of four-fold counts at the the detectors of our experiment were found to be of order 1 count per second.

6.1.1 Input State Preparation

Pairs of coinciding photons were coupled into optic fibres at the source using fibre couplers, and directed to the experiment which was located in an adjacent room. "Bat ear" polarisation controllers we used to rotate the polarisation of photons entering the circuit to as near horizontal (with respect to the optical table) as possible. Polarising beam splitters discarded all photons which were not horizontally polarised before they entered the circuit, defining a basis. The polarisation of each input beam was determined using half-wave plates, allowing us to prepare any arbitrary linear polarisation.

6.2 Detection And Measurement Of Output States

Successful operation of the circuit is detected as a coincident pair of photons arriving at the output arms of the circuit. For the CNOT, this entails one photon in the target output arm, and one in the control output arm. The measurement apparatus of each arm consists of a full polarisation analyser, a fibre-coupler, and an avalanche photodiode.

The polarisation analyser consists of a quarter-wave plate, a half-wave plate, and a polarising beam-splitter, in that order. This arrangement allows statistical analysis of polarisations to be performed on the output of the device by rotating a photon's polarisation by a predetermined amount and counting how often the photon is detected within a given time period.

Output beams are coupled into single-mode fibres, ensuring correct beam modes can be found and reducing erroneous background counts. Photons are detected by a pair of avalanche photodiodes, specifically two Perkin-Elmer SPCM-AQR-14-FC modules. An EG&G/Ortec 567 TAC/SCA was

used to detect coincident photon detections within a window of 5 ns. A GPIB controlled EG&G/Ortec 974 Quad Counter/Timer counted photon detections and coincidences.

This combination of optical components ensured that measurements could be performed in any polarisation basis. Full state tomography [28], which is the process of reconstructing states by measuring repeated instances of the state in a measurement basis that spans the space of density matrices, can be performed over a statistically significant sample of operations of the gate, signified by the number of coincident counts found in the detectors.

A similar arrangement is used for the USD. Two couplers are used to capture the $|\psi_?\rangle$ and $|\psi_\pm\rangle$ results. A linear-polarisation analyser consisting of a half-wave plate and a polarising beam splitter is used to distinguish $|\psi_+\rangle$ and $|\psi_-\rangle$ measurements. This allowed us to detect the three results of the USD. Statistical samples of each USD output were taken.

The limited number of available photon detectors meant that conclusive and inconclusive state statistics had to be measured separately. To change from performing state analysis of the $(|\psi_+\rangle, |\psi_-\rangle)$ basis to measuring $|\psi_?\rangle$ it was necessary to unplug the optic fibre of one coupler from the photo-detector, and plug in the fibre from the other coupler.

6.3 The Quantum Circuit

The complete quantum circuit (omitting the photon source) is illustrated in detail in Figure 6.2. It realises the CNOT and USD presented in previous sections, with the USD coupled to the target output of the CNOT circuit. It employs three classical interference and one HOM interference phenomena. The function of the CNOT and USD parts were tested independently before the complete circuit was characterised.

6.3.1 Achieving Hong-Ou-Mandel Interference

To assemble the CNOT gate it was necessary to align optical components such that a HOM dip could be achieved. To establish the condition of indistinguishability in photons necessary for a HOM dip, the input beams were aligned using translation stages and orientation mounts. Peaking the alignment was done in two steps.

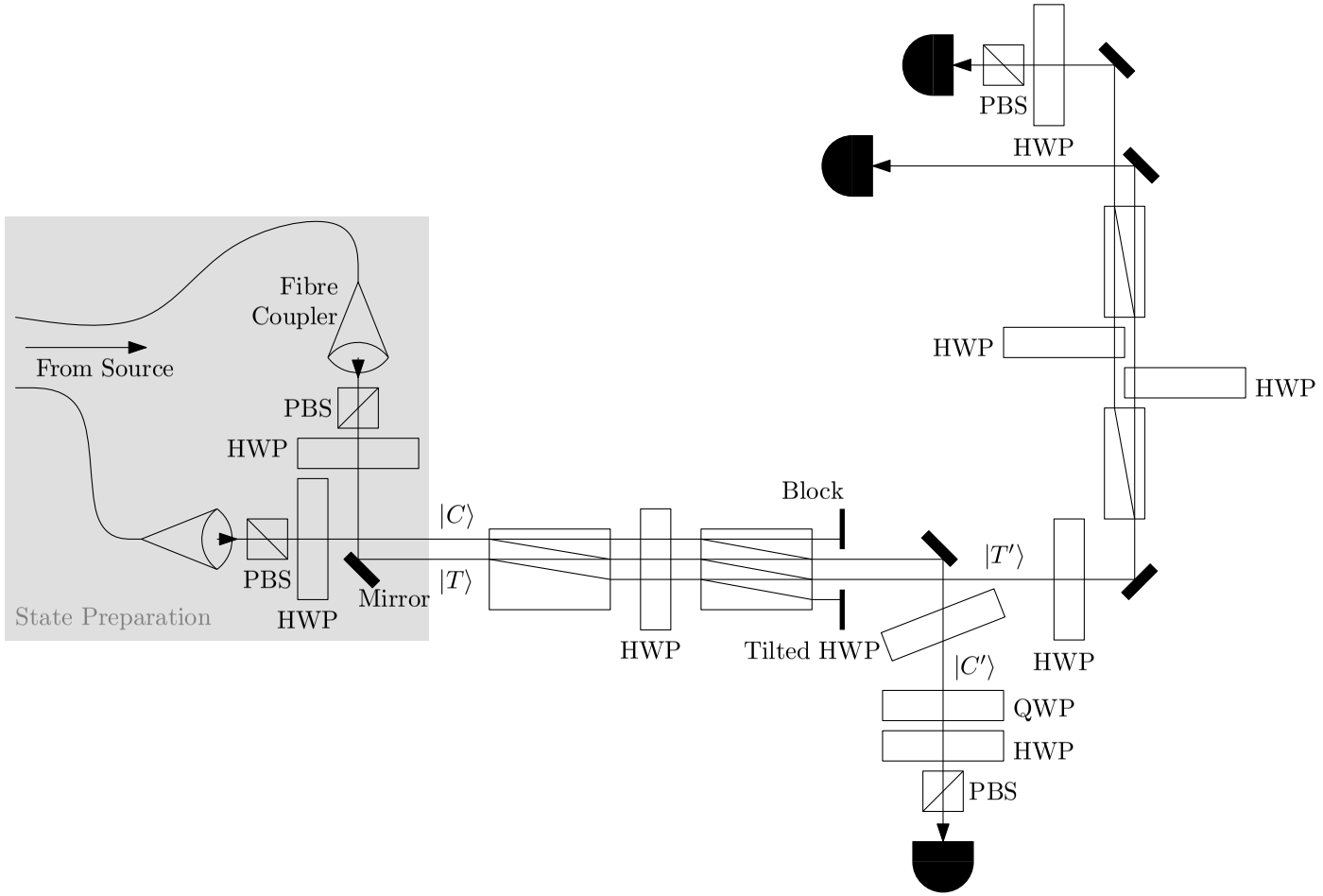

Figure 6.2: Layout of the entire QND-USD circuit. Inputs to the CNOT arrive from the photon source via optic fibres and have polarisations prepared by half-wave plates (HWPs). The CNOT circuit then operates on those inputs. The target output of the CNOT $|T'\rangle$ flows straight into the input of the USD circuit, while the control output $|C'\rangle$ is analysed by a standard polarisation analysis circuit.

First, before HOM interference can be established, the classical interferences were established and peaked. With a single input beam, any non-zero rotation of the beam displacers about the vertical axis causes a relative phase change in the two paths. This is just a classical interferometer with a relative difference in path length.

The CNOT circuit consists of two such classical interferometers. To make sure the displacers were aligned correctly we used a diagonally polarised beam as an input to one of the two arms, and looked for a high contrast of diagonal and antidiagonal in the output by rotating one beam displacer around the vertical axis. The point where the contrast is highest is where the relative rotation of the two displacers is zero. We achieved a classical interference contrast of 96%.

The other classical interferometer could not also be peaked by rotating the beam displacer in this way since this degree of freedom is fixed by the balancing of the first interferometer. An extra wave plate at its optic axis but tilted around the vertical axis is used to add an effective path length difference between the horizontal and vertical polarisations of photons after the beam displacers. This allows us to correct any path length difference in the beam displacers by rotating the waveplate around the vertical axis. Doing this we achieved a 97% contrast ratio.

For the second stage of alignment, a diode laser was used to align the inputs. One input was blocked and fibre couplers were used to capture the output beams into two single-mode optic fibres. The positions and orientations of the fibre couplers were then fixed. The block was then removed and placed onto the other input. The output beams were then made to couple into the same two fibres by moving and rotating the position of the input. Since single-mode fibres are very selective of position and orientation of beams, by having both inputs coupled to single-mode fibres at the same time ensured that the beams travelled the same paths, and this in turn ensured that the modes at the beam displacer where HOM interference takes place were identical.

Theoretically, if both output beams from one input are coupled, when one output beam from the other input couples the other output beam should also couple at the same time. This was not observed to be the case, with more efficient coupling observed to be partly independent in each coupler for the movable input. This may have been a result of beam displacers

being slightly different lengths (possibly due to the displacers having come from different batches) but we were unable to test this hypothesis. Instead, we peaked the coupling efficiency of the output beams due to the movable input simultaneously as best we could. The best efficiency of coupling that could be achieved on each output beam was roughly 62% in one coupler, and about 70% in the other couplers.

The condition of coincidence at the site of the quantum interference required the length of the paths the photons travelled in each beam to be equal. To achieve this, variable path length was added to one of the input arms by way of a pair of fibre couplers and a moving stage. One of the couplers was attached to the stage, the other was fixed to the table. As the stage moved, the separation between the couplers, and thus the length of the path travelled by that photon changed. As the path length difference approached zero, the HOM dip became evident. Scans over the path length were taken at various stages of evolution of the experiment, with typical visibilities of 90–97% before correction for erroneous four-fold counts. An example scan can be seen in Figure 6.3.

During the assembly and testing of the circuit it was discovered that the HOM interference was quite temperature sensitive. An apparent problem with the air-conditioning system meant that the ambient temperature in the lab oscillated by a few degrees over a forty minute interval. Coupled with the lengths of optic fibres between the source and the experiment, this resulted in the position of the variable path length stage needing to be changed regularly as the difference in path lengths oscillated with temperature.

6.3.2 CNOT Logical State Analysis

Data was taken with the circuit in the form shown in Figure 3.3 on page 28, that is, before the addition of components for the USD. Figure 6.4 shows the result of the ideal operation of the CNOT (6.4(a)) and the measured operation (6.4(b)). Probabilities for the measured states are listed in Table 6.1.

The measured results for $|00\rangle$ and $|01\rangle$ input states are very near the ideal case, with only minor variation likely due to four-fold counts. The results for $|10\rangle$ and $|11\rangle$ states have more error. This extra error is expected, and is likely due to imperfect HOM interference, caused by inexact beam overlap and changes in the arrival times of photons due to the influence of thermal fluctuations in the lab.

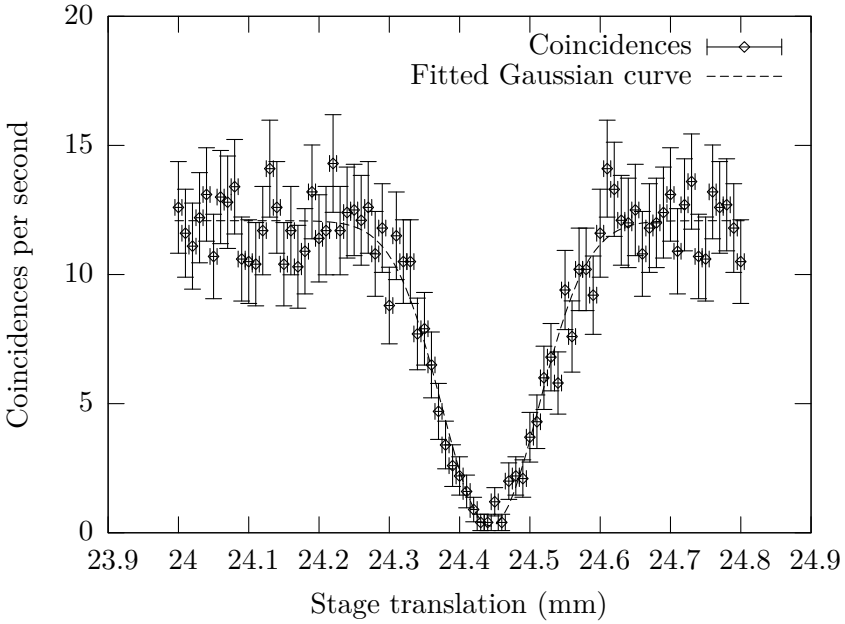

Figure 6.3: Observed Hong-Ou-Mandel interference. As the separation between photon path lengths changes, the difference in arrival times decreases, and a decrease in the number of coincident photon detections in the pair of output modes decreases. This HOM dip has a visibility of 98.1%, uncorrected for four-fold counts.

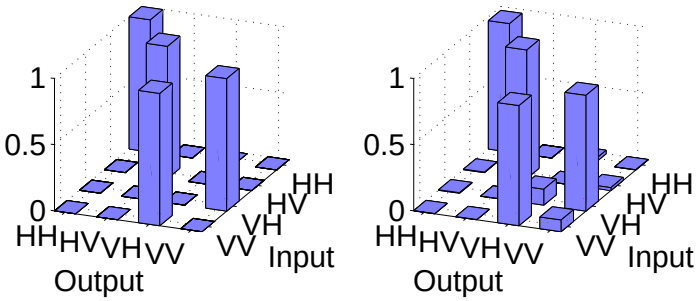

(a) Truth table of an ideal CNOT operation.

(b) Truth table of the realised CNOT gate.

Figure 6.4: Ideal and measured CNOT truth table. For the given pair of input states the CNOT operation produces the given ratios of output states. Our gate demonstrates almost ideal operation for H control input states, and only small deviation from ideal operation for V control input states.

Input	$P(\|00\rangle)$	$P(\|01\rangle)$	$P(\|10\rangle)$	$P(\|11\rangle)$
$\|00\rangle$	0.97126^a	0.00000	0.02709	0.00164
$\|01\rangle$	0.00446	0.97237^b	0.00089	0.02228
$\|10\rangle$	0.00398	0.00080	0.12102	0.87420^c
$\|11\rangle$	0.00164	0.00164	0.90789^d	0.08882

Table 6.1: Measured CNOT truth table. Rows represent input pairs, while columns represent probabilities of obtaining output pairs. For a given input state, the realised CNOT has the shown probability of returning a given output state. The truth table fidelity [2] is defined as $(a+b+c+d)/4$, and in this case is 0.93143.

6.3.3 CNOT Entanglement Analysis

To demonstrate the entanglement operation of the circuit a state of $|AD\rangle = \frac{1}{2}(|HH\rangle + |HV\rangle - |VH\rangle - |VV\rangle)$ was input and 2-qubit state tomography was performed on the output. The input state logically corresponds to a $|-0\rangle$ (footnote[3]) input for a CNOT, which when passed through a CNOT produces the maximally entangled state $\frac{1}{\sqrt{2}}(|00\rangle - |11\rangle)$.

Taking into account the missing Hadamard gate on the target output and the state flip on the control output, the state we expect to get out of this circuit is the maximally entangled state shown in Figure 6.5(a). The measured state is plotted in Figure 6.5(b).

The measured state was found to have a purity of 0.71 ± 0.03, a linear entropy of 0.38 ± 0.04, a tangle [29] of 0.53 ± 0.06, a trace distance from the ideal of 0.23 ± 0.03 and a fidelity with the ideal of 0.81 ± 0.02. These results indicate that, while the purity of states the gate produces is just okay (we surmise imperfect HOM interference is responsible for this), it is an entangling gate with results not far from ideal. There is a rotation in the resulting state likely due to an imbalance in one or both of the classical interferometers. We expect that with the addition of single-qubit unitary transforms a closer approximation to the ideal output could be achieved.

6.3.4 USD Analysis With Unentangled Single-Qubits

Extra components were added to the circuit to implement the USD device, and data was taken with the circuit in the form shown in Figure 6.2 on page 53 with the control input blocked. The circuit is then equivalent to

[3] $|-0\rangle = |-\rangle|0\rangle = \frac{1}{\sqrt{2}}(|0\rangle - |1\rangle)|0\rangle = \frac{1}{\sqrt{2}}(|00\rangle - |10\rangle)$

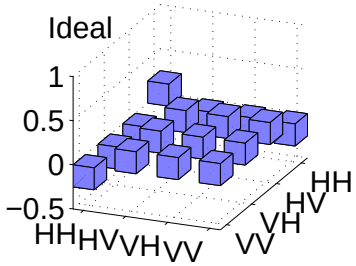

(a) Real part of the density matrix of the output state corresponding to an ideal CSIGN operation on $|AD\rangle$. The imaginary part is 0.

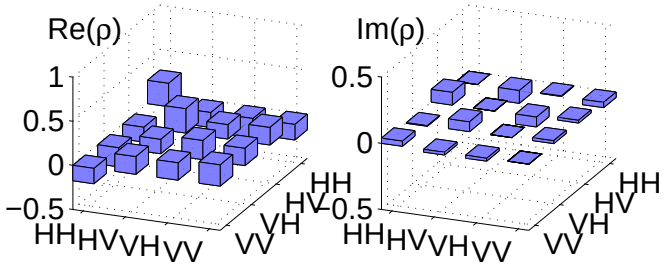

(b) Measured real and imaginary parts of the density matrix of the output state corresponding to the presented CSIGN gate operating on $|AD\rangle$.

Figure 6.5: Density matrices of the output state corresponding to the ideal and realised CSIGN gate operation on $|AD\rangle$.

Input	USD Output	Ideal Prob.	Measured Prob.
$\|\psi_+\rangle$	D	0.2929	0.2556 ± 0.0004
	A	0	0.0050 ± 0.0002
	Inconclusive	0.7071	0.7395 ± 0.0006
$\|\psi_-\rangle$	D	0	0.00065 ± 0.00007
	A	0.2929	0.2519 ± 0.0004
	Inconclusive	0.7071	0.7475 ± 0.0005

Table 6.2: Characterisation of USD measurements of unentangled nonorthogonal states. For the given input state, the output state had the listed probability of being measured.

that in Figure 5.1 on page 45.

The $|\psi_+\rangle$ and $|\psi_-\rangle$ states were chosen to be 45° apart and centered around V; the $|\psi_+\rangle$ state being 22.5° and the $|\psi_-\rangle$ state being −22.5° from V. Then we expect to receive inconclusive results with probability $1/\sqrt{2}$.

Single counts of photons exiting the USD circuit in A and D polarisations in the conclusive arm, simultaneously with V polarisations in the inconclusive arm, were taken over 10 s intervals and normalised. By blocking the input and performing the same process, accidental and background counts, primarily due to thermal effects in the detectors, were found to be a significant contribution to overall counts. These background counts have been deducted from the raw data, and the results are plotted in Figure 6.6. The ideal probabilities and measured probabilities are shown in Table 6.2.

This shows the USD circuit is operating in a near ideal manner, though the probability that this circuit heralds an inconclusive result is slightly higher than ideal, and the probability of a conclusive correct result slightly lower. The difficulty in rotating the wave plates held in place by clamps meant that this was the best result possible. With some mechanism to allow finer precision in wave plate rotation this result may be improved further.

The probability of obtaining an incorrect conclusive result (assuming a conclusive result) was 1.9% for an input of $|\psi_+\rangle$ and 0.2% for $|\psi_-\rangle$, both much lower than the Helstrom minimum error for these states, 14.6%. We conclude the USD circuit is operating successfully.

6.3.5 USD Analysis Of QND Entanglement

With both the CNOT and USD components operating correctly, the two circuits were joined so that the target output of the CNOT circuit fed into the

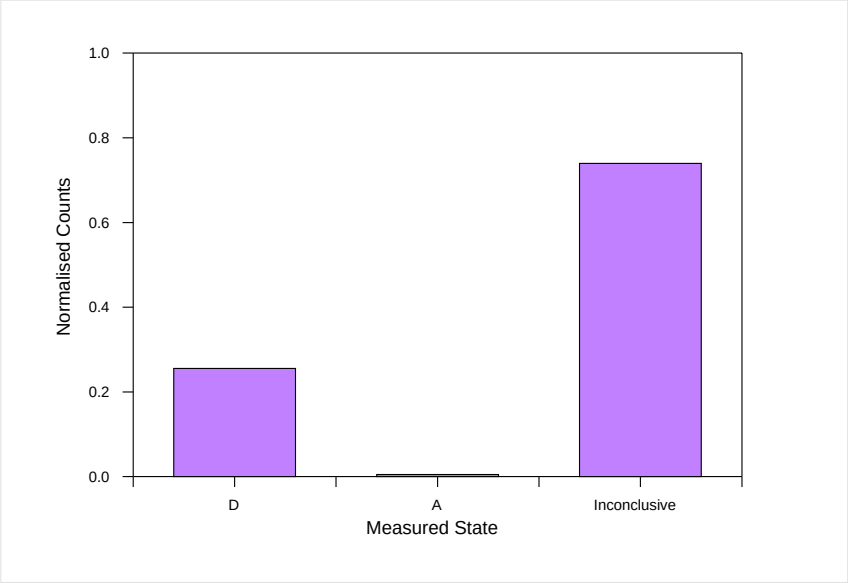

(a) Normalised counts of output states of the USD device with an input state $|\psi_+\rangle$.

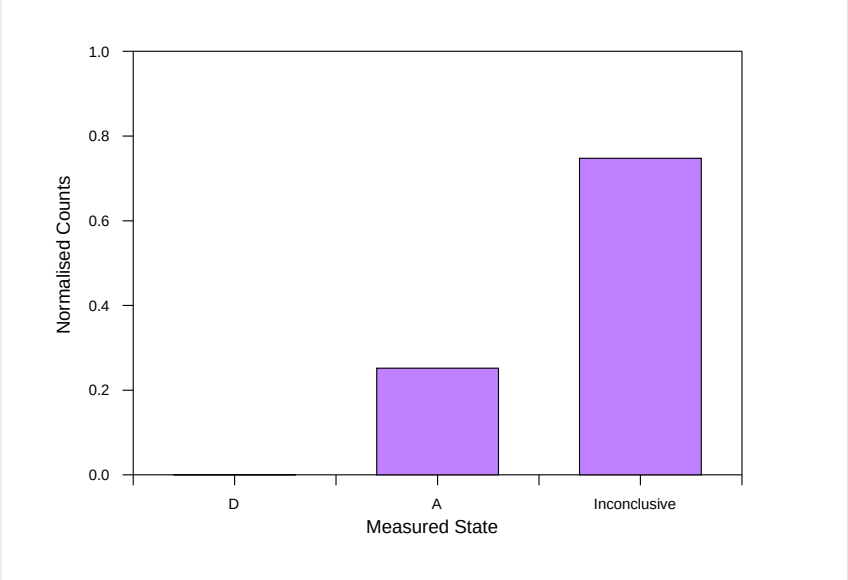

(b) Normalised counts of output states of the USD device with an input state $|\psi_-\rangle$.

Figure 6.6: USD measurements of unentangled nonorthogonal states. Shown are the normalised measured probabilities of obtaining the given result for each of the two non-orthogonal input states. In each case, the result D represents a successful measurement of the $|\psi_+\rangle$ state, while the result A represents a successful measurement of the $|\psi_-\rangle$ state.

input of the USD circuit. The control was set to input states $|\psi_+\rangle$ ($+22.5°$ from V) first, then $|\psi_-\rangle$ ($-22.5°$ from V), as the signal. The target was set so that entanglement occurred and full-strength QND could be performed on the signal state.

The USD device serves as a measurement on the target output, resulting in one of three outcomes. Single-qubit tomography and state reconstruction was performed on the control for each USD measurement outcome.

6.3.5.1 Strong QND Measurements

For strong QND, the target was set to D, equivalent to $|0\rangle$ for a CNOT. A and D measurements in the USD arm were taken over periods of 100 s for each of the six control arm measurements. Measurements of the $|\psi_?\rangle$ state, which had considerably more counts, were taken over 40 s. Measurements were also performed with identical settings, but one of each input arm blocked to obtain estimates of four-fold counts which contribute undesirably.

Topographic state reconstructions of each input, output, with four-folds included and removed were performed, with the results shown in Figures 6.7 to 6.12 on pages 62–65. Table 6.3 on page 65 lists the characteristics of the density matrices calculated.

As with the CNOT, we see a rotation of the measured state vector compared to the ideal, likely due to imperfect classical interference. Again we suppose that the addition of single-qubit unitary transforms could be used to obtain a closer approximation to the expected state.

We expect that half of the time a conclusive measurement is made, D is the result, and the other half, A. Then, instead of the ratio of the number of counts found in the correct state being 0.2929 and the incorrect state being 0 as for the case for unentangled single-qubit USD, we expect the ratio to be split evenly between the two. This means that for these input states we expect a ratio of D results equal to the ratio of A results and 0.1464, while the ratio of inconclusive results remains the same at 0.7071.

What we see, and is listed in Table 6.4, are ratios quite close to the ideal. As was the case for analysis of the use of USD on unentangled single-qubits, we see that the ratio of inconclusive results is a little higher than expected, by about 6%. Also, the conclusive counts are lower, by as much as 18% in the worst case (with input $|\psi_-\rangle$). However, this discrepancy is mostly due to the increase in the inconclusive results. The ratio of A and D results,

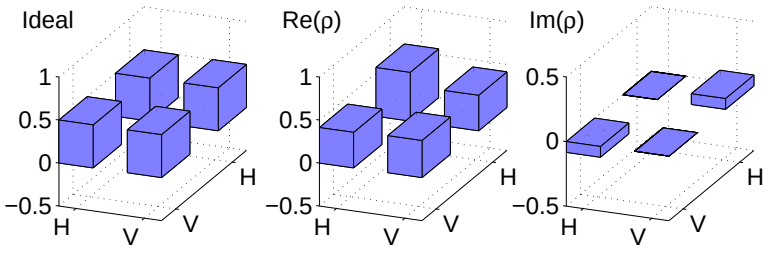

(a) Including four-fold counts.

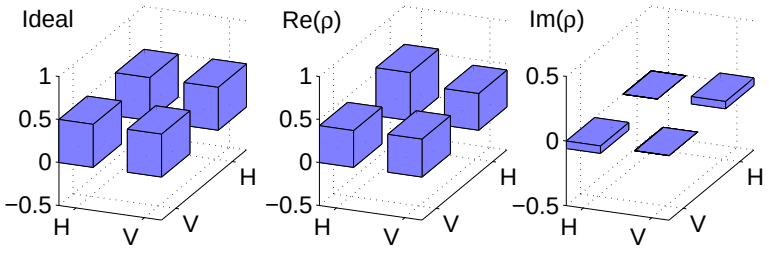

(b) Corrected for four-fold counts.

Figure 6.7: Density matrix for strong QND-USD measurements corresponding to the $|\psi_+\rangle$ input with D USD output. The top row of plots represents the measured state according to unadjusted counts. The bottom row represents the state determined after adjustments to compensate for erroneous four-fold coincidence events. Plotted is the real part of the density matrix for the ideal case (which has 0 imaginary component), and the real and imaginary components of the density matrix of the actual measured state.

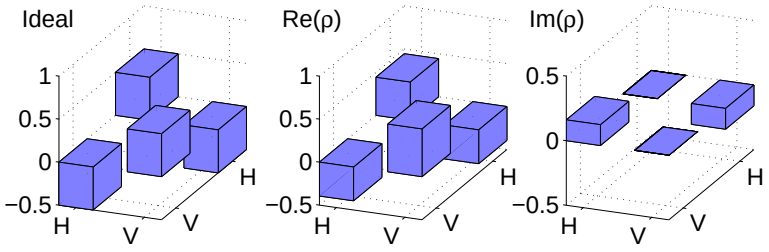

(a) Including four-fold counts.

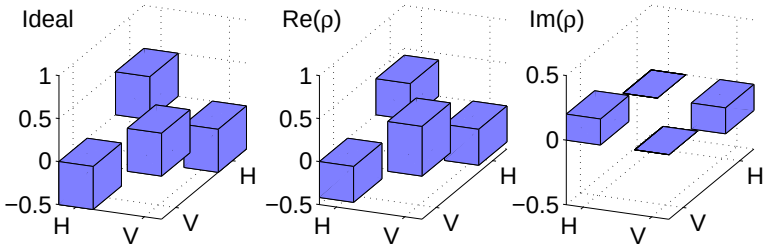

(b) Corrected for four-fold counts.

Figure 6.8: Density matrix for strong QND-USD measurements corresponding to the $|\psi_+\rangle$ input with A USD output. The ideal case has 0 imaginary component.

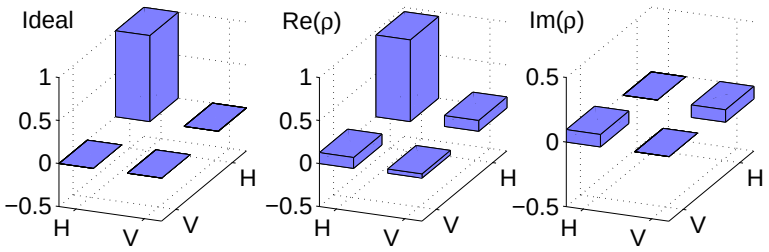

(a) Including four-fold counts.

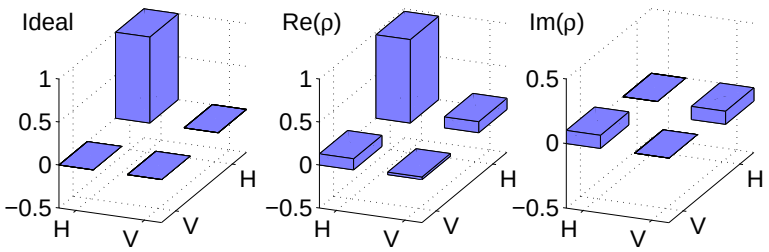

(b) Corrected for four-fold counts.

Figure 6.9: Density matrix for strong QND-USD measurements corresponding to the $|\psi_+\rangle$ input with inconclusive USD output. The ideal case has 0 imaginary component.

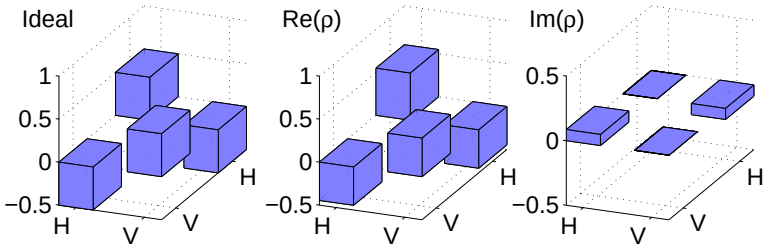

(a) Including four-fold counts.

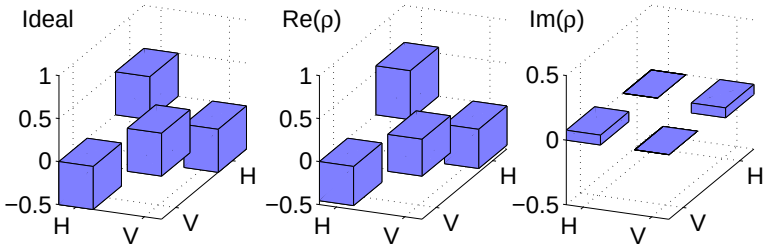

(b) Corrected for four-fold counts.

Figure 6.10: Density matrix for strong QND-USD measurements corresponding to the $|\psi_-\rangle$ input with D USD output. The ideal case has 0 imaginary component.

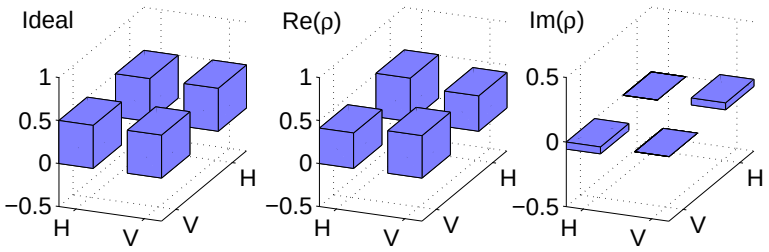

(a) Including four-fold counts.

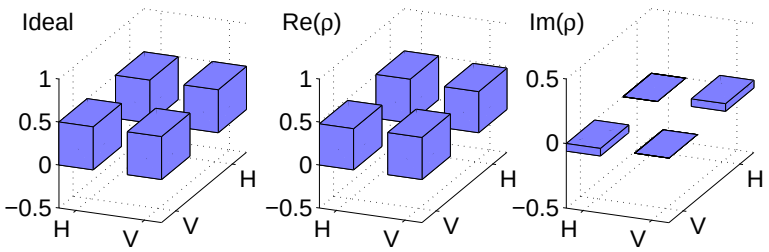

(b) Corrected for four-fold counts.

Figure 6.11: Density matrix for strong QND-USD measurements corresponding to the $|\psi_-\rangle$ input with A USD output. The ideal case has 0 imaginary component.

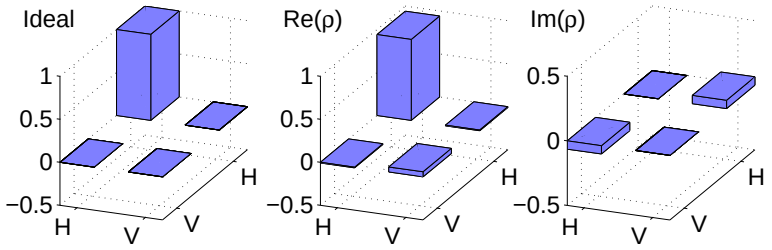

(a) Including four-fold counts.

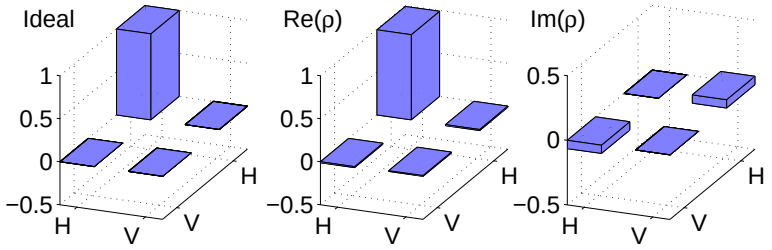

(b) Corrected for four-fold counts.

Figure 6.12: Density matrix for strong QND-USD measurements corresponding to the $|\psi_-\rangle$ input with inconclusive USD output. The ideal case has 0 imaginary component.

(a) Including four-fold counts.

Input	USD Output	Ideal	Trace Dist.	Purity	Lin. Entropy
$\|\psi_+\rangle$	D	D	0.14 ± 0.03	0.86 ± 0.03	0.27 ± 0.05
	A	A	0.20 ± 0.03	0.87 ± 0.03	0.26 ± 0.05
	Inconclusive	H	0.17 ± 0.02	0.96 ± 0.02	0.09 ± 0.04
$\|\psi_-\rangle$	D	A	0.11 ± 0.03	0.92 ± 0.03	0.17 ± 0.05
	A	D	0.10 ± 0.02	0.85 ± 0.03	0.31 ± 0.05
	Inconclusive	H	0.09 ± 0.02	0.90 ± 0.02	0.21 ± 0.03

(b) Corrected for four-fold counts.

Input	USD Output	Ideal	Trace Dist.	Purity	Lin. Entropy
$\|\psi_+\rangle$	D	D	0.11 ± 0.02	0.88 ± 0.03	0.24 ± 0.05
	A	A	0.23 ± 0.03	0.94 ± 0.03	0.12 ± 0.06
	Inconclusive	H	0.17 ± 0.02	1.00 ± 0.02	0.01 ± 0.03
$\|\psi_-\rangle$	D	A	0.11 ± 0.03	0.94 ± 0.03	0.13 ± 0.05
	A	D	0.06 ± 0.03	0.96 ± 0.02	0.07 ± 0.04
	Inconclusive	H	0.07 ± 0.02	0.989 ± 0.007	0.02 ± 0.02

Table 6.3: Characterisation of strong QND-USD measurements. Listed are the input states, measured USD output, expected control output, trace distance of the expected and measured control output states, purity and linear entropy of measured output states.

(a) Including four-fold counts.

Input	D Ratio	A Ratio	Inconclusive Ratio
$\|\psi_+\rangle$	0.1380	0.1500	0.7120
$\|\psi_-\rangle$	0.1188	0.1351	0.7416

(b) Corrected for four-fold counts.

Input	D Ratio	A Ratio	Inconclusive Ratio
$\|\psi_+\rangle$	0.1376	0.1457	0.7167
$\|\psi_-\rangle$	0.1196	0.1313	0.7491

Table 6.4: Ratios of USD outcomes for strong QND-USD measurements. Listed for each input state are the ratios of coincidence counts to the total for each USD measurement outcome. In every case, the ratio of D and A are ideally 0.1464, and the ratio of the inconclusive result is ideally 0.7071.

which should be 1, is at most 1.098 (also $|\psi_-\rangle$).

6.3.5.2 Weak QND Measurements

To perform weak QND measurements it is necessary that the meter qubit M be between $|0\rangle$ and $\frac{1}{\sqrt{2}}(|0\rangle + |1\rangle)$. We choose to perform weak measurements using the meter state half way between, i.e. $\cos 22.5° \,|0\rangle + \sin 22.5° \,|1\rangle$. This state is obtained by setting the target input wave plate to its optic axis plus 11.25°.

As for strong QND measurements, A and D measurements in the USD arm were taken over periods of 100 s each, while measurements of the $|\psi_?\rangle$ state were taken over 50 s and extrapolated.

Tomographic state reconstructions were performed, resulting in Figures 6.13 to 6.18 on pages 67–69. The characteristics of the reconstructed states are listed in Table 6.5. It is evident that when the USD device finds the D state, the state of the signal is near H. This means that the use of the simple filter mechanism would not work.

Table 6.6 lists the ratios of the number of normalised total counts for each USD outcome for each input. We can see that the D state, which signals the $|\psi_+\rangle$ measurement, is at least 3 times more likely to be observed than the A state, regardless of which non-orthogonal input state is used.

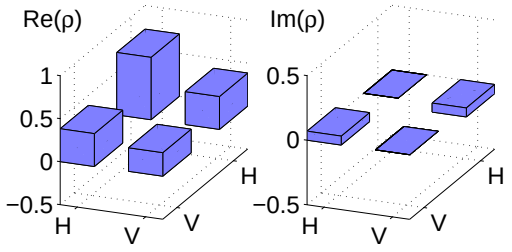

(a) Including four-fold counts.

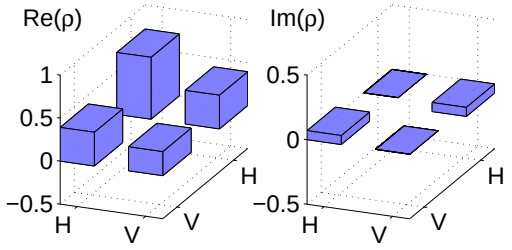

(b) Corrected for four-fold counts.

Figure 6.13: Density matrix for weak QND-USD measurements corresponding to the $|\psi_+\rangle$ input with D USD output. The top row of plots represents the measured state according to unadjusted counts. The bottom row represents the state determined after adjustments to compensate for erroneous four-fold conincidence events. Plotted is the real and imaginary components of the density matrix of the measured state.

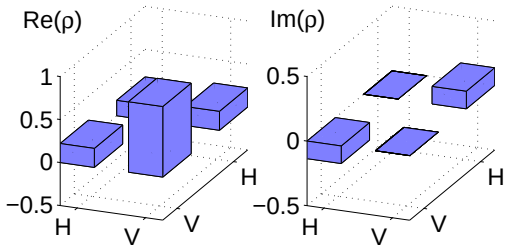

(a) Including four-fold counts.

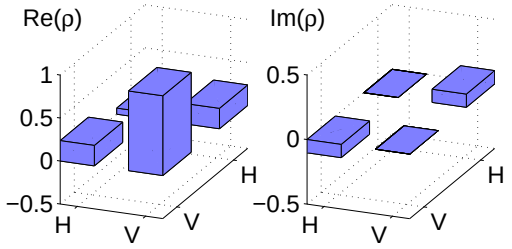

(b) Corrected for four-fold counts.

Figure 6.14: Density matrix for weak QND-USD measurements corresponding to the $|\psi_+\rangle$ input with A USD output.

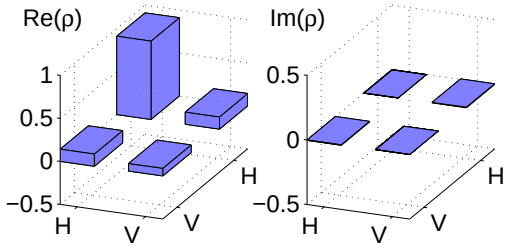

(a) Including four-fold counts.

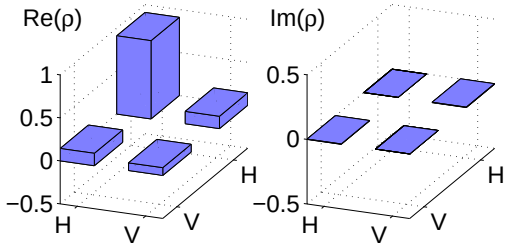

(b) Corrected for four-fold counts.

Figure 6.15: Density matrix for weak QND-USD measurements corresponding to the $|\psi_+\rangle$ input with inconclusive USD output.

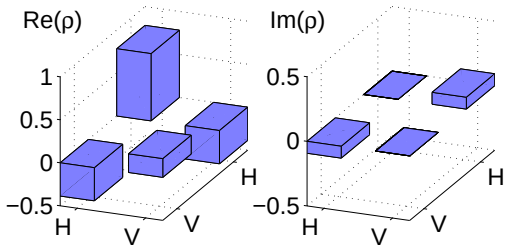

(a) Including four-fold counts.

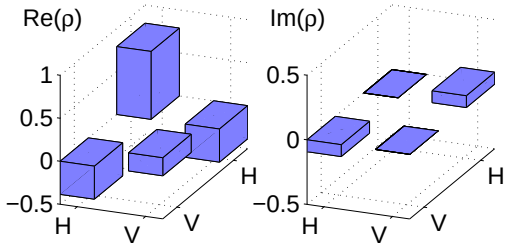

(b) Corrected for four-fold counts.

Figure 6.16: Density matrix for weak QND-USD measurements corresponding to the $|\psi_-\rangle$ input with D USD output.

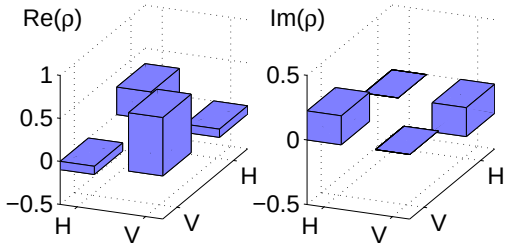

(a) Including four-fold counts.

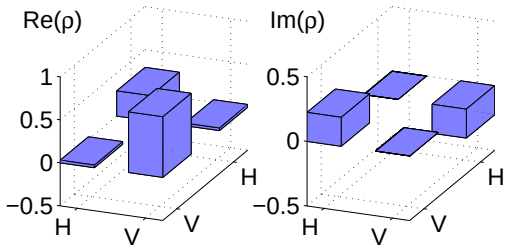

(b) Corrected for four-fold counts.

Figure 6.17: Density matrix for weak QND-USD measurements corresponding to the $|\psi_-\rangle$ input with A USD output.

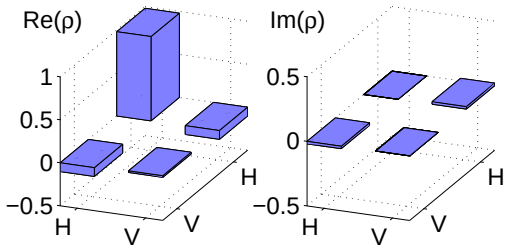

(a) Including four-fold counts.

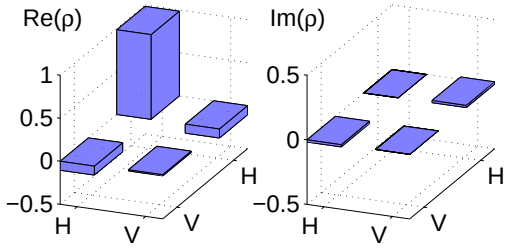

(b) Corrected for four-fold counts.

Figure 6.18: Density matrix for weak QND-USD measurements corresponding to the $|\psi_-\rangle$ input with inconclusive USD output.

(a) Including four-fold counts.

Input	USD Output	Purity	Lin. Entropy
$\|\psi_+\rangle$	D	0.90 ± 0.03	0.19 ± 0.06
	A	0.84 ± 0.06	0.3 ± 0.2
	Inconclusive	0.88 ± 0.02	0.24 ± 0.04
$\|\psi_-\rangle$	D	0.97 ± 0.03	0.05 ± 0.06
	A	0.68 ± 0.07	0.6 ± 0.2
	Inconclusive	0.98 ± 0.01	0.03 ± 0.02

(b) Corrected for four-fold counts.

Input	USD Output	Purity	Lin. Entropy
$\|\psi_+\rangle$	D	0.91 ± 0.04	0.17 ± 0.07
	A	1.00 ± 0.04	0.00 ± 0.07
	Inconclusive	0.88 ± 0.02	0.25 ± 0.04
$\|\psi_-\rangle$	D	0.98 ± 0.03	0.04 ± 0.05
	A	0.69 ± 0.07	0.6 ± 0.2
	Inconclusive	0.993 ± 0.008	0.014 ± 0.002

Table 6.5: Characterisation of weak QND-USD measurements. Listed are the input states, measured USD output, purity and linear entropy of measured output states.

(a) Including four-fold counts.

Input	D Ratio	A Ratio	Inconclusive Ratio
$\|\psi_+\rangle$	0.2570	0.0949	0.6481
$\|\psi_-\rangle$	0.2873	0.0561	0.6566

(b) Corrected for four-fold counts.

Input	D Ratio	A Ratio	Inconclusive Ratio
$\|\psi_+\rangle$	0.2607	0.0877	0.6516
$\|\psi_-\rangle$	0.2888	0.0504	0.6608

Table 6.6: Ratios of USD outcomes for weak QND-USD measurements. Listed for each input state are the ratios of coincidence counts to the total for each USD measurement outcome.

6.4 Discussion Of Results

Before combining them, we investigated the CNOT gate and the USD measurement device separately, as discussed in Sections 6.3.2–6.3.4. The CNOT gate has a truth table fidelity (i.e. fidelity of operations on logical states) of 0.93. This is quite close to the ideal, and is comparable to previous CNOT realisations [7, 13].

The density matrices resulting from the entangling operation by the gate showed a degree of state vector rotation away from the expected result and some mixture. We believe that the rotation is caused by imperfectly balanced classical interferometers, i.e. phase shifts in the interferometer of roughly 5 degrees. This might be addressed by better balancing or by the addition of single qubit rotations after the gate.

It should also be noted that that lab had atypically large temperature fluctuations (up to ± 2 degrees C) with a period of about 40 minutes, such that the phase varied between when the interferometer was set and when data was taken. This isn't typical for the lab — temperature fluctuations of ± 0.5 degrees C maximum are expected, and phase rotations are not expected to be a dominant source of noise.

Modelling suggests the mixture in the state is most likely caused by imperfect HOM interference [7, 13, 24]. We typically achieved HOM interference visibilities between 90 and 97%.

Despite the imperfection of the gate, the entanglement we observed was sufficient for continuation of the experiment. We expect to see a similar degree of rotation and mixture in the results of analysis of the circuit once the CNOT gate is combined with the USD device.

The operation of the USD device on single-qubit inputs proved to be close to what was expected. The ratio of inconclusive results to the total was, for both inputs, about 5% higher than the ideal case, however the ratio of incorrect discriminations to correct ones was very low, less than 2%, and much lower than the minimum error possible with a Helstrom measurement.

It is possible that the ratio of inconclusive results is affected by the difficulty in accurately adjusting the waveplates that are held in clamps in the USD circuit, though we might expect that the ratio of incorrect discriminations to correct ones would rise if this were the case. A possible explanation for the higher inconclusive counts is better fibre coupling in that

particular output mode. In any case, we concluded that the USD device was operating successfully within reasonable bounds.

The combination of the CNOT gate and the USD device that implemented the QND-USD apparatus produced signal states that had strong correlation with the USD measurement result, within the strong QND regime. For example, the measurement for the input state $|\psi_+\rangle$ shown in Figure 6.7. Here we expect to see correlation between the signal and USD outcome such that a measurement of D by the USD circuit, signalling the $|\psi_+\rangle$ result, guarantees a D state in the signal.

By performing single-qubit tomography on the signal for each USD result we can assess how close the state we actually observe is to what we expect it to be. We expect that for perfect operation, the purity of states should be 1, and the trace distance (a measure of how different two states are) between the measured state and the expected state should be zero.

For each USD measurement result the final state of the signal was found to be close to what was expected, however rotation and mixture, which we expected to see from the imperfections in the CNOT gate, was present. This meant that the purity of the resulting signal density matrices of each USD output measurement was lowered (due to imperfect HOM operation and beam overlap in the CNOT), and the trace distance from the ideal was higher (due to imperfect classical interference in the CNOT).

In principle, the addition of single-qubit unitary transformations after the CNOT could decrease the trace distance between the measured and expected states. The important thing to consider is how orthogonal the output state of the signal for the D USD measurement is to the output state of the signal for the A USD measurement. For orthogonality, the trace distance between the two states must be 1. It was found that the trace distances between these two states for $|\psi_+\rangle$ input was 0.89 and for $|\psi_-\rangle$ input was 0.95, both corrected for four-fold counts. It is clear that, while not perfect, these results mean that the signal output states are quite orthogonal for different conclusive USD measurement results, and so the addition of single-qubit unitary transformations to rotate those states to ideal is feasible.

It is important to note the implications of the degree of orthogonality of the signal output states on the filtering mechanism necessary to make this non-demolition unambiguous discriminator work. For the false state filter

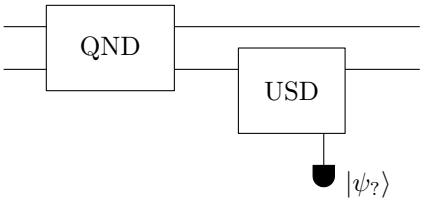

Figure 6.19: Block diagram representing the combination of CNOT and USD devices. Note that there is a detector only on the inconclusive result. To characterise this circuit, two-qubit state tomography is performed on the signal and conclusive outputs, making the results conditional on not detecting the inconclusive result.

to work it needs to operate on signal output states that are orthogonal, since non-orthogonal states will sometimes be filtered incorrectly. States that represent true operation of the USD and are only almost-orthogonal to the states that represent false operation may sometimes be measured by the filter as being false states.

To improve the purity of the state, however, the imperfection of the HOM interference would need to be addressed. Theoretical analysis of the circuit with imperfect HOM mode matching [25] suggests that the impurities in the resulting signal states (including the atypically low A purity for the $|\psi_-\rangle$ input) are expected for HOM interference visibilities of around the level we achieved, usually above 90%. Although fibre coupling has produced good HOM interference, future developements might include realisations of circuits entirely within waveguide devices, which should improve HOM visibility.

In addition to its operation as a single-qubit measuring device, our circuit should perform a two-qubit controlled-nonunitary operation, taking each of two non-orthogonal states to corresponding orthogonal Bell states, conditional on not observing the inconclusive outcome of the USD (see Figure 6.19). Our results above, which show the correct correlations in the D/A basis, are consistent with this interpretation of the circuit operation, within acceptable bounds. However, to show that this is indeed the operation performed would require measurement in other bases (such as full two-qubit tomography) to be performed on the signal output and the conclusive outputs of the USD. Work to perform these measurements is currently underway.

Attempts to perform weak measurements were unsuccessful. The reason for this is as follows. For strong measurements, in the case of a conclusive USD result, the CNOT entangles the meter and signal qubits. The USD operation on the meter in this entangled state produces identical probabilities for each conclusive result of the USD, however the signal collapses to a state that can be used in a filtering mechanism. For weak QND measurements the CNOT only partially entangles the meter and signal qubits. The resulting two-qubit state has an entangled part and a separable part. The entangled part contains information about the state of the signal, but the separable part contains no such information.

It turns out that the separable part of the weak QND operation biases the statistics of the USD measurement, and changes the signal output state such that the filter would no longer work correctly. We found that irrespective of which non-orthogonal input was used, the probability of obtaining a D USD result was much greater than the probability of obtaining an A USD result, and that irrespective of which non-orthogonal input was used, a D USD result gives a signal state close to H. No information about the state of the signal input can be drawn from such results, even when the measurement strength is not zero. Thus our attempt to naïvely perform weak QND-USD measurements in the same manner as weak projective QND measurements was unsuccessful.

It should be noted that other configurations of the circuit, such as varying the internal settings of the USD device or changing the measurement basis, may allow some information to be extracted from a weak measurement. However, this extension requires additional theoretical modelling, which is beyond the scope of this project.

6.5 Future Directions

What we have demonstrated with this experiment is probabilistic QND orthogonalisation (in the cases where we did not get the inconclusive USD outcome) of an input qubit which is in one of two non-orthogonal states. Unfortunately, the resulting orthogonal states are the entangled states $|DD\rangle + |AA\rangle \equiv |HH\rangle + |VV\rangle$ and $|AD\rangle + |DA\rangle \equiv |HH\rangle - |VV\rangle$. As it stands, the circuit is unable to discriminate states of the input signal without some sort of operation involving the signal photon after it leaves the QND device.

We have found that, in order to successfully unambiguously and non-destructively discriminate the state of the signal qubit, we need to use some sort of filter mechanism. The simplest filter suggested diverts signal states that represent false results and, upon detection, flags an incorrect USD measurement. In the event that such a signal state is not detected, the device has worked successfully, and the signal photon could then continue to the hypothetical next part of a circuit, as would be the case for regular a QND measurement. This filter mechanism rejects 50% of conclusively discriminated inputs due to the fact that obtaining a true or false result is random with equal probability. Also, the mechanism is always successful only if the photo-detector has 100% efficiency. If successful discrimination occurs, a feed-forward mechanism, like that by Pittman et al [22], after the filter would be necessary to rotate the signal back to its original state.

A more sophisticated mechanism which would work 100% of the time would be to use an additional QND measurement on the signal output in the D/A basis. Since the states D and A are orthogonal, an ideal CNOT gate could perform this QND measurement with certainty. With the addition of a second QND device, the state of the signal can be determined for all cases where the USD result was conclusive, and so the truth or falsehood of the conclusive USD result can be found.

A feed-forward mechanism would again be necessary to rotate the signal to its original state. For example, if the USD outcome is $|\psi_+\rangle$ and the signal is measured to be D by the second QND device, then the input must have indeed been $|\psi_+\rangle$. In this case the feed-forward system would need to rotate the signal from D to $|\psi_+\rangle$. However, if instead of D the signal was found in the A state, the input would have actually been $|\psi_-\rangle$, and the feed-forward would need to rotate the signal from A to $|\psi_-\rangle$. Note that this option of employing a second QND device now requires two entangling operations[4].

A third and more elegant mechanism comes from recognising that we essentially wish to distinguish entangled states, and so what we require is a *non-local* filter similar to Bell state measurement. Such a filter would take the partially entangled states after the QND circuit, and with conclusive USD operations, result in the separable states $|\psi_+\rangle|\psi_+\rangle$ or $|\psi_-\rangle|\psi_-\rangle$. A proposed circuit capable of this (due to Tim Ralph) has construction and operation similar to a CNOT gate, but it would have a different HOM

[4] And an additional ancilla qubit for the meter of the second QND device.

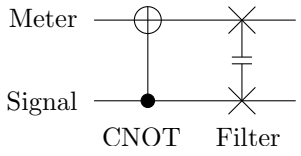

Figure 6.20: Advanced QND-USD filter mechanism that produces separable states, assuming conclusive USD results. The filter is very similar to the CNOT gate and appears immediately after it.

reflectivity parameter, which is dependent on the angle between the two non-orthogonal states being discriminated. It appears just after the CNOT as shown in Figure 6.20.

We could use this device on the signal and meter after the QND operation, resulting in separable but correlated signal and meter output states. These states are much easier to discriminate between than the entangled states from the CNOT QND device by itself. A USD operation on the meter part of the $|S'M'\rangle = |\psi_+\rangle\,|\psi_+\rangle$ or $|\psi_-\rangle\,|\psi_-\rangle$ states will never yield a false result, and being a separable state, no back-action on the signal will occur, so this scheme would not even require a feed-forward mechanism.

It is interesting to note that both the second QND and non-local filter mechanisms similarly require at least two entangling gates. This suggests that 2 may be the lower limit of the number of entangling gates necessary to perform QND-USD with 100% efficiency, and it raises the idea of a general exploration of resources necessary for different classes of generalised measurements. An understanding of what resources are required to implement various advanced measurements is at least as important for practical applications as an understanding of what those advanced measurements are capable of.

Both of these advanced filter schemes require two 2-qubit entangling gates, one following the other. The scheme involving a second QND device can be achieved using the same coincidence-heralded linear optics gates that we have presented in this thesis. The 2-qubit filter scheme, however, cannot be done in linear optics using coincidence-heralded gates. A failure of the first gate may result in two photons in one of its output modes, and as these photons then go through the filter they might split up, moving to each of that gate's two output modes. This would flag as a successful operation even though the first gate had failed.

The process is very similar to the problem of four-fold events from the source which we have already addressed, however the likelihood of failure of the first gate means that the size of this problem would overwhelm true results. Other more complicated linear optics gates exist where this is not a problem [3]. A two-QND circuit does not have this problem since it is heralded on coincidence of three photons — the signal and two meter photons.

It is also interesting to note that the circuit presented generates orthogonal maximally entangled states from non-orthogonal states. This is a novel entangling operation that has yet to be completely characterised, though it is worth noting that there are similarities with the entanglement distillation experiment of Kwiat et al [30], where filtering is also used to generate maximally entangled states.

Chapter 7

Conclusion

Understanding quantum measurements gives us knowledge of the fundamental possibilities and limitations of quantum information, and allows us to devise schemes and devices that have promising applications in quantum computation, control, and telecommunications. By investigating the properties of advanced quantum measurement systems we get insight into the issues surrounding some of the more non-trivial and counter intuitive aspects of quantum mechanics.

Previously, examples of advanced quantum measurement devices, including QND and USD, have been shown individually. QND has presented us with schemes for measuring qubit states in the logical basis without destuction via quantum entanglement, while USD has given us insight into the operation of POVM measurements, demonstrating measurements with more than two outcomes, and performing unambiguous discrimination of non-orthogonal states.

The QND device works using a CNOT gate, a two-input gate that flips one input conditional on the state of the other input. With a CNOT gate it is possible to perform strong QND, where full information about an input system is obtained, and weak QND, where only partial information about an input system is obtained with the benefit of decreased back-action if the input was not in the logical basis. The CNOT gate is also capable of generating maximally entangled states and performing Bell state measurements.

We have presented an experimental realisation of an optical CSIGN gate in the polarisation basis. We have shown that a CSIGN gate is equivalent to a CNOT gate to within single-qubit unitary transformations. The realisation

presented is non-deterministic, heralded by coincident detection of photons.

The gate employs two classical interferometers and a quantum interference effect known as Hong-Ou-Mandel interference, where indistinguishable photons bunch into common modes. Classical interference visibilities of over 95%, and HOM interference visibilities of over 98% were achieved. We then demonstrated the gate to be functioning with logical basis input states with fidelity 0.93%, and the tangle and fidelity of a Bell state produced by the gate was found to be 0.53 ± 0.06 and 0.81 ± 0.02, respectively. The fidelity may be higher overall since we did not perform full quantum process tomography on the gate.

A USD device capable of discriminating between non-orthogonal states without error was also described. The theoretical measurement operations were presented in terms of POVM measurement and element operators, and shown to result in three measurement outcomes, two representing states, and a third representing an inconclusive result. This inconclusive result accounts for all the uncertainty in the non-orthogonality of the two states.

The effect of using the USD device on entangled states was investigated theoretically, and it was discovered that, although performing USD on the meter output of the QND operation orthogonalised both the meter and the signal qubit, it was not sufficient to make any determination. We showed that it is necessary to perform a measurement or some sort of filter on the signal to determine the truth or falsehood of a discrimination operation. Different solutions involving filtering the output of the QND of the signal were presented.

We then detailed an optical device for unambiguously discriminating polarisations. The device attempts to orthogonalise non-orthogonal states by diverting some common polarisation to another mode. This mode heralds the inconclusive state. The device was shown to work using input states centered around the vertical polarisation and 45° apart with less than 6% error in inconclusive counts, and less than 2% error in conclusive discriminations.

The combination of both experimental devices was then explored. We have shown that it is possible to unambiguously and non-destructively discriminate an input from being one of two non-orthogonal states. Our circuit does this, assuming successful CNOT operation, with 50% probability. We have discussed how it is in principle possible to do this with 100% probability by employing a second QND or CNOT-like device.

The device presented exhibits strong QND discrimination of non-orthogonal states with purity typically better than 94% and trace distance from ideal typically less than 0.17. A rotation of state vector common to all results was found caused by imperfect classical interference. The resulting states appear strongly correlated between the input state and the output result of the USD.

We have also shown that attempting to perform weak USD measurements in the same manner as weak projective measurements does not work. We demonstrated this using meter states half-way between a strong QND measurement and no measurement, $|M\rangle = \cos 22.5^\circ |0\rangle + \sin 22.5^\circ |1\rangle$. While we found purities typically greater than 80%, the output states appear to have little correlation to the input state.

In conclusion, we have successfully demonstrated a proof-of-principle implementation of a device that unambiguously discriminates an input as being in one of two non-orthogonal quantum states without demolition. The number of common-mode elements make this circuit tricky to assemble in practice, but it has been successful as a tool to explore some aspects of general quantum measurements. We have seen that one of the biggest key issues in advanced measurement is the effects of entanglement that produce results that go against intuition. Undoubtedly, it is this counter-intuitiveness that will become the basis for advanced technologies based on quantum information theory in the future.

Bibliography

[1] Nicolas Gisin, Grégoire Ribordy, Wolfgang Tittel, and Hugo Zbinden. Quantum cryptography. *Reviews of Modern Physics*, 74(1):145–195, March 2002.

[2] Michael A. Nielsen and Isaac L. Chuang. *Quantum Computation and Quantum Information*. Cambridge University Press, 2000.

[3] E. Knill, R. Laflamme, and G. J. Milburn. A scheme for efficient quantum computation with linear optics. *Nature*, 409:46–52, 2001.

[4] Robert Raussendorf and Hans J. Briegel. A one-way quantum computer. *Physical Review Letters*, 86(22):5188–5191, May 2001.

[5] Philippe Grangier, Juan Ariel Levenson, and Jean-Philippe Poizat. Quantum non-demolition measurements in optics. *Nature*, 396:537, December 1998.

[6] B. Huttner, A. Muller, J. D. Gautier, H. Zbinden, and N. Gisin. Unambiguous quantum measurement of nonorthogonal states. *Physical Review A*, 54(5):3783, November 1996.

[7] J. L. O'Brien, G. J. Pryde, A. G. White, T. C. Ralph, and D. Banning. Demonstration of an all-optical quantum controlled-NOT gate. *Nature*, 426:264–267, November 2003.

[8] G. J. Pryde, J. L. O'Brien, A. G. White, S. D. Bartlett, and T. C. Ralph. Measuring a photonic qubit without destroying it. *Physical Review Letters*, 92(19), May 2004.

[9] Roger B. M. Clarke, Anthony Chefles, Stephen M. Barnett, and Erling Riis. Experimental demonstration of optimal unambiguous state discrimination. *Physical Review A*, 63(4):040305, March 2001.

[10] Paul Horowitz and Winfield Hill. *The art of electronics.* Cambridge University Press, second edition, 1989.

[11] T. C. Ralph, S. D. Bartlett, J. L. O'Brien, G. J. Pryde, and H. M. Wiseman. Quantum nondemolition measurements for quantum information. *Physical Review A*, 73(012113), January 2006.

[12] C. K. Hong, Z. Y. Ou, and L. Mandel. Measurement of subpicosecond time intervals between two photons by interference. *Physical Review Letters*, 59(18):2044–2046, November 1987.

[13] J. L. O'Brien, G. J. Pryde, A. Gilchrist, D. F. V. James, N. K. Langford, T. C. Ralph, and A. G. White. Quantum process tomography of a controlled-NOT gate. *Physical Review Letters*, 93(8), August 2004.

[14] Christopher C. Gerry and Peter L. Knight. *Introductory Quantum Optics.* Cambridge University Press, 2005.

[15] Rodney Loudon. *The Quantum Theory Of Light.* Oxford University Press, third edition, 2000.

[16] Tamyka B. Bell. Non-classical interference in quantum logic circuits. Honours thesis, University of Queensland, 2002.

[17] T. C. Ralph, N. K. Langford, T. B. Bell, and A. G. White. Linear optical controlled-NOT gate in the coincidence basis. *Physical Review A*, 65(062324), June 2002.

[18] Eugene Hecht. *Optics.* Addison-Wesley, second edition, 1987.

[19] C. W. Helstrom. *Quantum Detection and Estimation Theory.* Academic Press, New York, 1976.

[20] I. D. Ivanovic. How to differentiate between non-orthogonal states. *Physics Letters A*, 123(6):257–259, August 1987.

[21] D. Dieks. Overlap and distinguishability of quantum states. *Physics Letters A*, 126:303, January 1988.

[22] T. B. Pittman, B. C. Jacobs, and J. D. Franson. Demonstration of feed-forward control for linear optics quantum computation. *Physical Review A*, 66(5):052305, November 2002.

[23] T. B. Pittman, B. C. Jacobs, and J. D. Franson. Demonstration of quantum error correction using linear optics. *Physical Review A*, 71(5):052332, May 2005.

[24] P. P. Rohde, G. J. Pryde, J. L. O'Brien, and T. C. Ralph. Quantum-gate characterization in an extended Hilbert space. *Physical Review A*, 72:032306, September 2005.

[25] Ben Lanyon. Personal communication. September 2006.

[26] Nathan Langford. Towards a linear optics CNOT gate ... or 'Twisted in cnots!'. Honours thesis, University of Queensland, 2001.

[27] H. Hellwig, J. Liebertz, and L. Bohatý. Exceptional large nonlinear optical coefficients in the monoclinic bismuth borate BiB_3O_6. *Solid State Communications*, 109(4):249–251, 1999.

[28] Joseph B. Altepeter, Daniel F. V. James, and Paul G. Kwiat. Qubit quantum state tomography. *Lecture Notes in Physics*, 649:113–145, 2004.

[29] Andrew G. White, Alexei Gilchrist, Geoffrey J. Pryde, Jeremy L. O'Brien, Michael J. Bremner, and Nathan K. Langford. Measuring controlled-NOT and two-qubit gate operation. arXiv:quant-ph/0308115, August 2003.

[30] Paul G. Kwiat, Salvador Barraza-Lopez, André Stefanov, and Nicolas Gisin. Experimental entanglement distillation and 'hidden' non-locality. *Nature*, 409:1014–1017, February 2001.